An M-Tech research report

on

SLIP FLOW IN MICROCHANNELS

In partial fulfilment of the requirement for the degree

of

Master of Technology

in

Thermal Engineering Specialization

by

Khan Rehan Wasim

(Roll No. 211ME3165)

Under the guidance of

Prof AK SATPATHY

Department of Mechanical Engineering National Institute of Technology Rourkela

An M-Tech research report

on

SLIP FLOW IN MICROCHANNELS

In partial fulfilment of the requirement for the degree

of

Master of Technology

in

Thermal Engineering Specialization

by

Khan Rehan Wasim

(Roll No. 211ME3165)

Department of Mechanical Engineering National Institute of Technology Rourkela

National Institute of Technology Rourkela

CERTIFICATE

This is to certify that the report entitled **"**SLIP FLOW IN MICROCHANNELS**"** submitted to the National Institute of Technology, Rourkela by **Khan Rehan Wasim**, Roll No. **211ME3165** in partial fulfillment of the requirement for the degree of **Master of Technology** in **Department of Mechanical Engineering** with specialization in **Thermal Engineering** is a record of bona fide work carried out by him under my supervision and guidance.

Place: NIT Rourkela, Date: June 03, 2013.

.

Prof AK SATAPATHY
Department of Mechanical Engineering
National Institute of Technology Rourkela.

TABLE OF CONTENTS

NOMENCLATURE

K	Thermal conductivity	Ts	Surface temperature
U	U-velocity	x	Length of microchannel
V	V-velocity	υ	Kinematic viscosity
μ	Viscosity		
ρ	Density		
C_p	Specific heat		
n	Normal direction		
L_s	Slip length		
Nu	Nusselt number		
Re	Reynolds number		
Pr	Prandtl number		
L	Length of microchannel		
b	Width of microchannel		
U_w	Slip velocity		
f	Friction factor		
τ	Shear stress		
P	Pressure		
T	Temperature		
q_s	Constant heat flux		

ABSTRACT

The assumption that a liquid adheres to a solid boundary ("no-slip" boundary condition) is one of the central tenets of the Navier-Stokes theory. However, there are situations wherein this assumption does not hold.One-dimensional single phase models for microchannel flow with slip flow boundary conditions have been presented here. The geometry of the problem and meshing of it have been made in GAMBIT. The simulation of steady incompressible fluid flow and heat transfer is done using ANSYS 13 FLUENT Software. Usually, the slip is assumed to depend on the shear stress at the wall.In the present work, the slip flow of liquid through a microchannel has been modeled using a slip length assumption instead of using conventional Maxwell's slip flow model, which essentially utilizes the molecular mean free path concept. The hydrodynamics and thermal behaviour of a rectangular microchannel are studied here. The variation wall temperature, pressure drop in the channel and the friction factors calculated using ANSYS Fluent can well predict the experimental data. The effect of Re on the behaviour the channel are also studied. The models developed, following this approach, lend an insight into the physics of liquid flow through microchannels. Initially, in order to study the physics of flow inside the microchannel a simple analysis was done in a circular pipe.

KEYWORDS: Microchannel; slip length; Hagen–Poiseuille; Nusselt number; friction factor

Chapter 1

INTRODUCTION

1.1 INTRODUCTION

Microfluidics is an area of science and engineering in which fluid behaviour differs from conventional flow theory primarily due to non-continuum effects, surface dominated effects, and low Reynolds number effects induced by the small length scale of the micro flow systems. With the recent achievements in the field of nanotechnology, microprocessor chip cooling, patterned drug delivery, and biotechnology, the microfluidic devices are becoming more prevalent both in commercial application and in scientific inquiry. The classification proposed by Mehendale and andlikar and Grande categorized the range from 1 to 100 μm as microchannels. In microfluidics, theoretical knowledge for gas flows is currently more advanced than that for liquid flows. Concerning the gas flow through microchannels, the issues are actually more clearly identified; the main micro effect that results from shrinking down of device size is 'rarefaction'. In the continuum fluid transport theory, governed by the Navier–Stokes equations, it is assumed that the state variables do not vary appreciably over the length and time scales compared with the molecular mean free path and molecular relaxation time. The local density oscillation near the solid–liquid interface of the microchannels, significant deviation of liquid viscosity compared with the bulk value, may not necessarily mean the breakdown of continuum theory; at the same time, it is important to understand how the continuum theory works in a micro flow. There were no evidences that continuum assumptions were violated for the microchannels tested, most of which had hydraulic diameters of 50 μm or more. There is a clear need for additional systematic studies that carefully consider each parameter influencing transport in microchannels. In general, there seems to be a paradigm shift in the focus of published articles from descriptions of the manufacturing technology to the discussions of the physical mechanisms of flow and heat transfer through microchannels Sobhan and Garimella have made a comprehensive review on investigations regarding the flow and heat transfer characteristics for microchannel flow.

Apart from wetting, adsorption, and electrokinetic effects, the slip phenomena play an important role in modelling liquid flow through microchannel. Helmloltz and Von Piotrowski found evidence of slip between a solid surface and a liquid and later Brodman verified their results. Navier (1823) was the first to model partial slip at the wall for liquids well before Maxwell's slip model for gases (1879). Slip length is the distance behind the solid–liquid interface at which the velocity extrapolates to zero. An interpretation of the slip length (Ls) is shown in fig1.1. The validation of slip boundary conditions continued in the beginning of the 20th century, with a focus mostly on flow through capillaries. Traube and Whang reported four-to fivefold increase in flow rate of water in a capillary treated with oleic acid. This increment could be attributed either to boundary slip or simply as surface tension-induced capillary rise. The systematic study undertaken by Schnell who used water in glass capillaries (240–800μm) treated with silicone to make them hydrophobic reported that for a small pressure drop in the capillary, the flow rate was lower in the treated cases compared with the untreated ones, but at the higher pressure drop, the experience was opposite. Moreover, with the onset of turbulence, there was no discernible difference in flow rates. Schnell's experiments stood the test of time and are considered as the first convincing proof of boundary slip occurring for water flow on hydrophobic surfaces. In the last few decades, there has been a renewed interest in determining the validity of the no slip boundary condition for liquids due to the interest in polymers and other complex fluids but primarily due to microfluidic applications. The effective use of the surface force apparatus (SFA) in the 1990s has led to many interesting experimental results and detailed studies of boundary slip with water and other substances. Liquid flow in a microchannel becomes fully developed after a short entrance length so that it can be modeled as a two dimensional flow. In view of this, present study aims for one-dimensional and two-dimensional microchannel flow simulation with non-continuum (slip velocity) boundary conditions, in general. The present

article is focused on analyzing the effect of two-dimensional dependency of velocity, compressibility of liquid flow through a microchannel on a simple analytical and computational fluid dynamics perspective. Majority of the experimental works indicate a strong dependence of the slip length on the approach rate (and thus shear rate) and wall roughness of the microchannels. Very large values of slip length of the order of hundreds of nanometers were reported in the open literature. Tretheway and Meinhart used microparticle image velocimetry (PIV) to measure the velocity profiles of water in 30 × 300 μm channel. The channel surfaces were treated with a 2.3-nm octedecyltrichlorosilane (OTS) layer. The velocity profiles were measured in a 25 × 100 μm plane to within 450 nm of the channel wall. A slip velocity of about 10% of the maximum velocity was measured, which corresponds to slip length of about 1 μm. This large value of slip length is typically encountered in polymer flows. Choi *et al* .(2003) reported slip length of 30 nm at the shear rate of 105 s−1 in OTS-coated 500-μm-wide × 9-mm-long microchannels of heights 0.5 and 1.0 μm. In case of hydrophilic surfaces of the same channels and for the same shear rate, they reported a slip length of 5 nm. Molecular dynamic (MD) simulation predicts the slip length to be roughly 1/10th of the experimental results. These large discrepancies have been addressed with the help of a few conceptual slip models like 'molecular slippage' model considered by Blake 'gaseous film' model proposed by Ruckenstein and Rajora 'viscosity model' proposed by Vinogradova and 'no shear/no-slip patterning' presented by Phillip. In the gaseous film model, it was assumed that there may be a film of gas at the interface between solid surface and liquid. The origin of this film may be the externally dissolved gases up to metastable concentrations. According to deGennes, this gas film nucleates bubbles preferentially near the wall at contact angles greater than 90◦,that is, on hydrophobic surfaces. Evidences of nanobubbles on a hydrophobic glass surface in water using atomic force microscope were reported by Tyrrell and Attard.Thickness of the gaseous film was assumed to be less than 0.5

nm. deGennes proposed a simple mathematical model for calculating slip length involving gaseous film thickness and physical properties of the fluid concerned and postulated a slip length of few microns for liquid flow through microchannel. The Viscosity model proposed by Vinogradova was inspired by the slip mechanism in polymer melts. It provides a relation between the slip length and a decrease in viscosity within a very thin boundary layer δ close to a hydrophobic surface. He proposed a model for slip length (slip length, $b = \delta[(\mu b/\mu s) - 1]$, where μb is bulk viscosityand μs is a near wall viscosity). According to him, there may be two mechanisms; instrumental for a large slip length, either large increment of δ or very high viscosity ratio. On the basis of the discussion so far about slip length, the authors think that in the present problem choosing a value of slip length as clearance length (b)/100 for micro flow simulation will not contradict any physical institution.Modeling the micro flows, especially for the gases require the mean molecular diameter d, the mean molecular spacing δ, and the mean free path λ. For dilute gases, d/λ is less than 1 and different collision models based on this assumption determine the value of λ that when divided by the channel characteristic length gives rise to a very important parameter Knudsen number for flows in microchannels. In the present work, the conventional

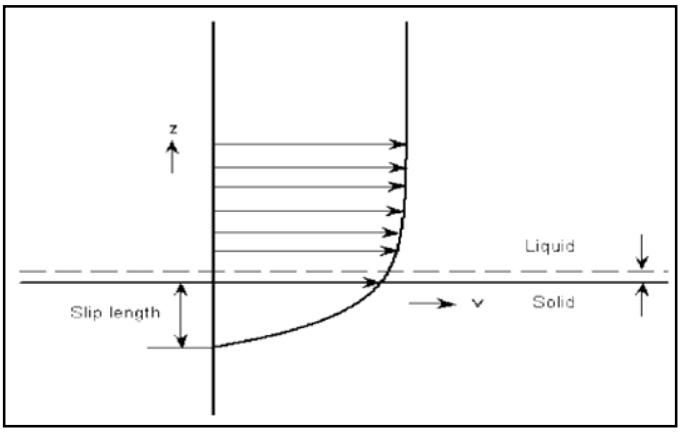

Fig.1.1 Slip length for slip flow of liquid on solid surface

Maxwell's slip flow model was not used, which essentially utilizes the mean free path, and does not require a slip length assumption. An analog to molecular mean free path, the molecular diffusive path has been proposed here using a slip length assumption to define a modified Knudsen number for liquid flow through microchannel.

1.2 MICROCHANNEL AND ITS USE

Tuckerman and Pease (1981) first made use of miniaturization for the purposes of heat removal, within the scope of a Ph.D. study in 1981. Their publication titled "High Performance Heat Sinking for VLSI" is credited as the first study on microchannel heat transfer. Their pioneering work has motivated many researchers to focus on the topic and microchannel flow has been recognized as a high performance heat removal tool ever since. Before proceeding with microchannel flow and heat transfer, it is appropriate to introduce a definition for the term "microchannel". The scope of the term is among the topics of debate between researchers in the field. Mehendale (2000) used the following classification based on manufacturing techniques required to obtain various ranges of channel dimensions,

"*D*", being the smallest channel dimension:

$1\mu m < D < 100\mu m$: Microchannels

$100\mu m < D < 1\ mm$: Minichannels

$1\ mm < D < 6\ mm$: Compact Passages

$6\ mm < D$: Conventional Passages

Microchannel heat sinks constitute an innovative cooling technology for the removal of a large amount of heat through a small area. It is one of the potential alternatives for replacing conventional finned tube heat exchangers, mainly used in industries such as automobiles, air conditioning and refrigeration at present. The heat sink is usually made from a high thermal conductivity solid such as silicon or copper with the micro-channels fabricated into its surface by either precision machining or micro-fabrication technology. A Micro-channel heat

sinks typically contains a large number of parallel micro channels. Coolant is forced to pass through these channels to carry away heat from a hot surface. In Micro channel heat exchangers flow is typically laminar and heat transfer coefficients are proportional to velocity. Micro-channel heat sinks provide very high surface area to volume ratio, large convective heat transfer coefficient, small mass and volume, and small coolant inventory. These attributes render these heat sinks very suitable for cooling devices such as high-performance microprocessors, laser diode arrays, radars, and high-energy-laser mirrors. Micro channel heat exchangers could be easier to repair than their conventional counterparts. It offers other benefits, including increased latent capacity for micro channel evaporators. Micro channel heat exchangers improve heat transfer in two ways. First, the smaller dimensions of the refrigerant flow passages increase refrigerant-side heat transfer. Second, the flat tube orientation reduces airside flow resistance, leading to either increased airflow or reduced fan power.

1.3Why Microchannels?

The heat transfer coefficient increases as channel size is decreased.

$$h_{avg} = 4.36\frac{k}{D_h}$$

There are two methods to increase the heat transfer coefficient, either to increase the thermal conductivity or decrease the diameter of the pipe. Since thermal conductivity is a property of the material it remains constant. Therefore to increase the heat transfer coefficient the diameter is decreased.

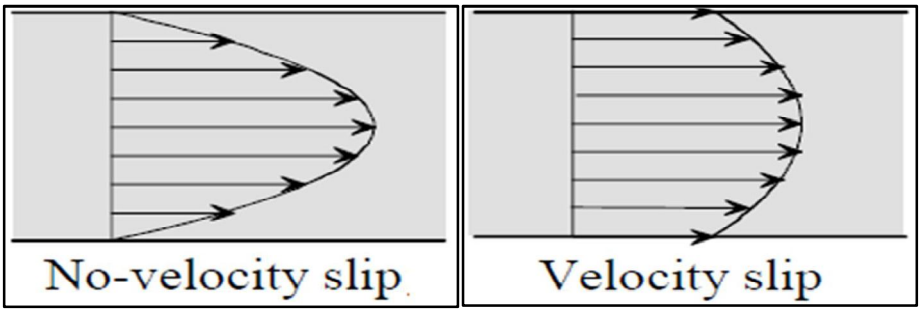

Fig 1.2 Velocity profile for Slip and No-slip

1.4 OUTLINE OF THE REPORT

Chapter 1 represents complete introduction of project work including definition of microchannel, application of it microchannel and its use, role of CFD and its application.

Chapter 2 is devoted on the extensive literature survey on topic namely experimental and theoretical development of the micro channel and the effect of slip flow in microchannel. In the theoretical survey, more emphasis is given on computational fluid dynamics (CFD) analyses of it.

Chapter 3 deals with simulation of single phase fluid flow in a circular micro channel. The effect of slip velocity on microchannel is implemented by UDF which express the shear stress in terms of pressure gradient. The variation of axial velocity is compared for microchannel and minichannel along with pressure. The Nusselt number is determined for the microchannel with slip flow and also for no-slip. The model equation includes the equation of continuity, momentum equation and energy equation.

Chapter 4 deals with the detailed explanation of Numerical method and CFD analysis using GAMBIT and ANSYS13 FLUENT of single phase flow in Microchannel with the effect of slip velocity at the walls.

Chapter 5 deals with result and discussion.

Chapter 6 deals with the overall conclusions and future recommendations.

Chapter 2

LITERATURE REVIEW

2.1 Introduction

The "no-slip" boundary condition is one of the cornerstones on which the mechanics of the linearly viscous liquid is built. In his original paper, Navier had proposed a slip boundary condition wherein the slip velocity depended linearly on the shear stress. Helmholtz and Pitrowski introduced the notion of the "coefficient of slip" (Gleitungskoeffizient) for the slip occurring adjacent to a wall. Kundt and Warburg studied the damping of a vibrating disk in a gas and found that the coefficient of slip was inversely proportional to the pressure. They also studied the flow of air and hydrogen in glass tubes and again found that the coefficient of slip was inversely proportional to the pressure. Later, Maxwell derived an expression for the slip of a gas next to a solid surface. A detailed discussion of the early work in this area can be found in Kennard. The "no-slip" boundary condition is also widely used for flows involving non-Newtonian fluids past solid boundaries. However, it has been found that a large class of liquid slip or stick-slip on solid boundaries. The slip velocity depends on the shear stress.

2.1.1NUMERICAL STUDY OF SLIP FLOW IN MICRO CHANNELS

M Kundu and **Dilip M** (2010) One-dimensional and two-dimensional models for microchannel flow with non-continuum (slip-flow) boundary conditions have been presented here. This study presents an efficient numerical procedure using pressure-correction-based iterative SIMPLE algorithm with QUICK scheme in convective terms to simulate a steady incompressible two-dimensional flow through a microchannel. In the present work, the slip flow of liquid through a microchannel has been modeled using a slip length assumption instead of using conventional Maxwell’s slip flow model, which essentially utilizes the molecular mean free path concept. The

models developed; following this approach lend an insight into the physics of liquid flow through microchannels.

2.1.2ANALYTICAL STUDY OF SLIP FLOW IN MICRO CHANNELS

Guyh and **Erchiqui** (2004) studied, the liquid flow with the slip boundary condition in a micro channel between two parallel plates with imposed heat flux was numerically investigated. The combined effect of pressure-driven flow and electro-osmosis was taken into account. Electric potential, liquid flow and thermal characteristics were determined using the Poisson–Boltzmann, the modified Navier–Stokes and the energy equations for a hydrodynamical and thermal steady fully developed laminar flow for an incompressible liquid. The results demonstrate the influence of the slip coefficient, the heat flux and the pressure difference on flow velocity, local temperature and Nusselt number. A comparison of the developed model results with those in a previous study was made.

2.1.3EXPERIMENTAL STUDY OF SLIP FLOW IN MICRO CHANNELS

Derek and **Meinharta** (2007) Micron-resolution particle image velocimetry is used to measure the velocity profiles of water flowing through 30x300 μm channels. The velocity profiles are measured to within 450 nm of the microchannel surface. When the surface is hydrophilic ‘uncoated glass’, the measured velocity profiles are consistent with solutions of Stokes’ equation and the well-accepted no-slip boundary condition. However, when the microchannel surface is coated with a 2.3 nm thick monolayer of hydrophobic octadecyltrichlorosilane, an apparent velocity slip is measured just above the solid surface. This velocity is approximately 10% of the free-stream velocity and yields a slip length of

approximately 1 μm. For this slip length, slip flow is negligible for length scales greater than 1 mm, but must be considered at the micro and nano scales.

Koo and **Clement** (2001) Experimental observations of liquid microchannel flows are reviewed and results of computer experiments concerning channel entrance, wall slip, non-Newtonian fluid, surface roughness, and viscous dissipation and turbulence effects on the friction factor are discussed. The experimental findings are classified into three groups. Group I emphasizes 'flow instabilities' and group II points out 'viscosity changes' as the causes of deviations from the conventional flow theory for macrochannels. Group III caters to studies that did not detect any measurable differences between micro- and macroscale fluid flow behaviors. Based on numerical friction factor analyses, the entrance effect should be taken into account for any microfluidic system. It is a function of channel length, aspect ratio and the Reynolds number. Non-Newtonian fluid flow effects are expected to be important for polymeric liquids and particle suspension flows. The wall slip effect is negligible for liquid flows in microconduits. Significant surface roughness effects are a function of the Darcy number, the Reynolds number and cross-sectional configurations. For relatively low Reynolds numbers, $Re < 2000$, onset to turbulence has to be considered important because of possible geometric non-uniformities, e.g., a contraction and/or bend at the inlet to the microchannel. Channel-size effect on viscous dissipation turns out to be important for conduits with $D_h < 100$ μm.

2.2 OBJECTIVES OF THE PRESENT WORK

As is evident from the diversity of application areas, the study of flow and heat transfer in microchannels is very important for the technology of today and the near future, as developments are following the trend of miniaturization in all fields. Literature shows that the microchannels with slip flow were studied extensively, but there is limited research related to the performance study of microchannel with slip flow using CFD models. Following from the experimental investigation of Guyh and Erchiqui (2007), this work studies the CFD simulation of micro channel flow and heat transfer, which couples fluid convection in a rectangular micro channel and heat conduction in the solids. The present work is undertaken to study the following aspects of Computational Fluid Dynamics modeling and simulation of single phase flow in micro channel with slip flow to understand its hydrodynamic and thermal behavior. Validation of the CFD models by comparing the present simulated results with the data available in the open literature.

Chapter 3

THEORY AND FORMULATION

THEORY AND FORMULATION

3.1 ONE-DIMENSIONAL FLOW THROUGH A CIRCULAR PIPE

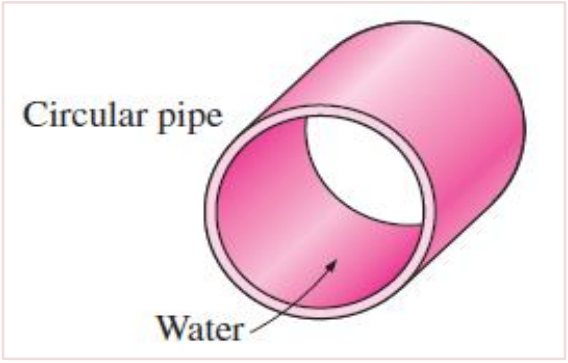

Fig 3.1 Liquid flow through a circular pipe

3.1.1 GENERAL THERMAL ANALYSIS

In the absence of any work interactions (such as electric resistance heating), the conservation of energy equation for the steady flow of a fluid in a tube can be expressed as

$$\dot{Q} = \dot{m}C_p(T_e - T_i) \qquad (3.1)$$

where Ti and Te are the mean fluid temperatures at the inlet and exit of the tube and Q is the rate of heat transfer to or from the fluid.

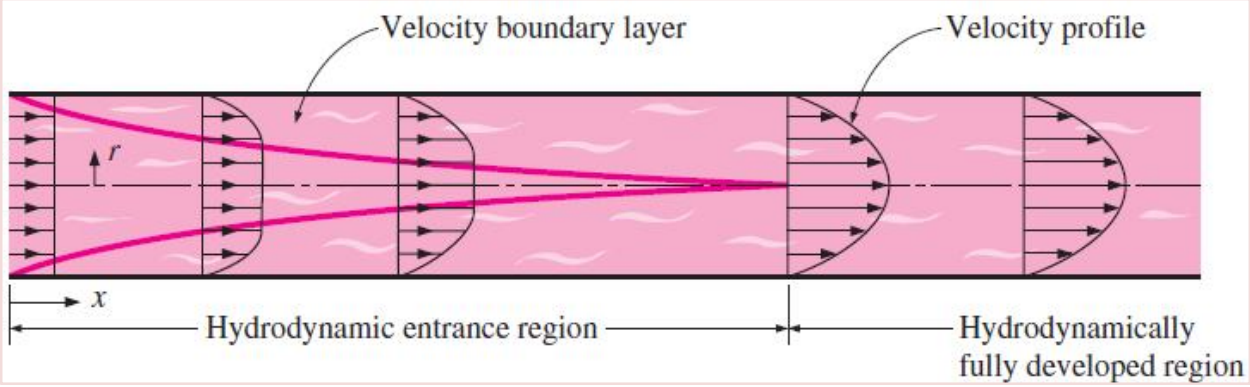

Fig 3.2 Velocity profile in pipe

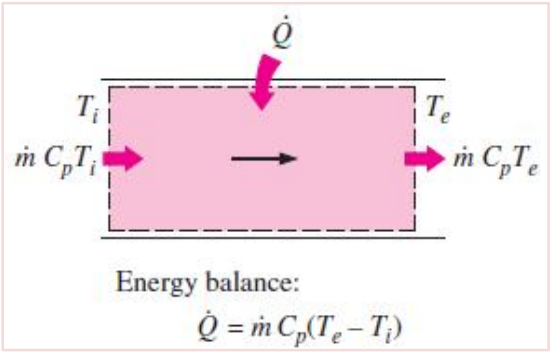

Fig 3.3 Energy balance across a fluid element

The thermal conditions at the surface can usually be approximated with reasonable accuracy to be constant surface temperature (T_s constant) or constant surface heat flux (q_s constant).

Surface heat flux is expressed as

$$q_s = h_x(T_s - T_m) \qquad (3.2)$$

Where hx is the local heat transfer coefficient and Ts and Tm are the surface and the mean fluid temperatures at that location.

3.1.2 Constant Surface Heat Flux (q_s Constant)

In this case of $q_{s=}$ constant the rate of heat transfer can also be expressed as

$$\dot{Q} = \dot{q}_s A_s = \dot{m} C_p (T_e - T_i) \qquad (3.3)$$

Then the mean fluid temperature at the tube exit becomes,

$$T_e = T_i + \frac{\dot{q}_s A_s}{\dot{m} C_p} \qquad (3.4)$$

The mean fluid temperature increases linearly in the flow direction in the case of constant surface heat flux, since the surface area increases linearly in the flow direction.

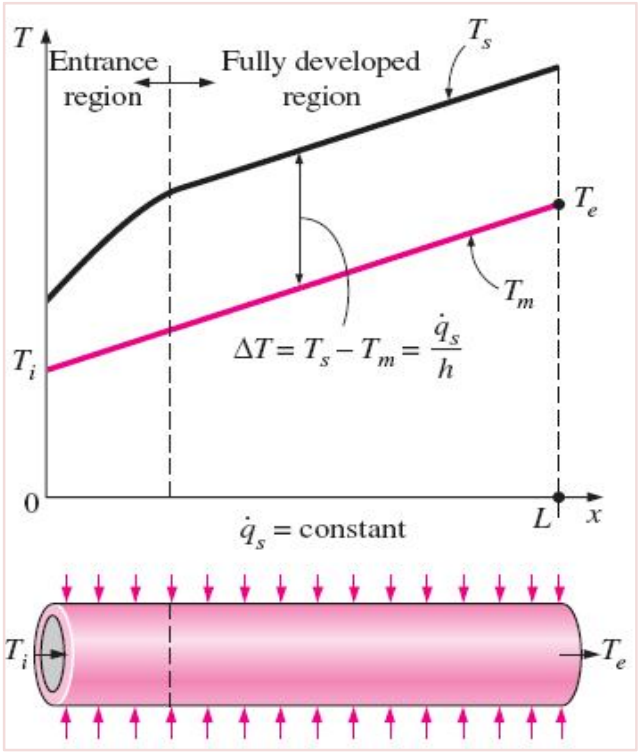

Fig 3.4 Variation of mean fluid temperature for isoflux condition

The surface temperature in the case of constant surface heat flux q_s can be determined from

$$T_s = T_m + \frac{q_s}{h} \qquad (3.5)$$

The slope of the mean fluid temperature Tm on a T-x diagram can be determined by applying the steady-flow energy balance to a tube slice of thickness dx as shown in Fig 3.5

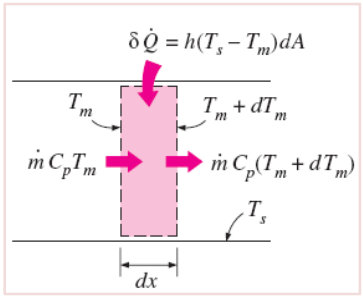

Fig 3.5 Energy balance across a mass of fluid for isoflux condition

The dimensionless temperature profile remains unchanged in the fully developed region gives

$$\frac{\partial T}{\partial x} = \frac{dT_s}{dx} = \frac{dT_m}{dx} = \frac{\dot{q}_s p}{\dot{m} C_p} = \text{constant} \qquad (3.6)$$

In fully developed flow in a pipe subjected to constant surface heat flux, the temperature gradient is independent of x and thus the shape of the temperature profile does not change along the tube.

3.1.3 Constant Surface Temperature (Ts constant)

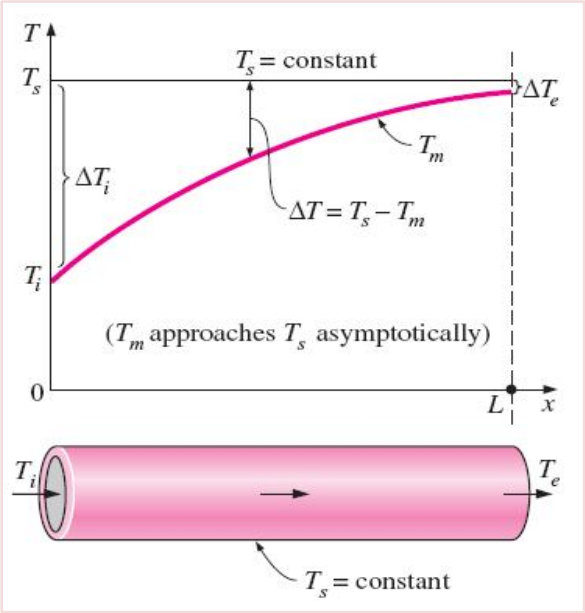

Fig 3.6 Variation of mean fluid temperature for isothermal condition

From Newton's law of cooling, the rate of heat transfer to or from a fluid flowing in a tube can expressed as

$$\dot{Q} = hA_s \Delta T_{ave} = hA_s (T_s - T_m)_{ave} \qquad (3.7)$$

Where h is the average convection heat transfer coefficient, as is the heat transfer surface area and T_{avg} is average temperature difference between the fluid and the surface. In the constant

surface temperature (Ts constant) case. Δ Tavg can be expressed approximately by the arithmetic mean temperature difference Δ Tam as

$$\Delta T_{\text{ave}} \approx \Delta T_{\text{am}} = \frac{\Delta T_i + \Delta T_e}{2} = \frac{(T_s - T_i) + (T_s - T_e)}{2} = T_s - \frac{T_i + T_e}{2}$$
$$= T_s - T_b \qquad (3.8)$$

Where Tb = (Ti -Te)/2 is the bulk mean fluid temperature.

The energy balance on a differential control volume shown in Fig 3.5 gives

$$\dot{m} C_p dT_m = h(T_s - T_m) dA_s \qquad (3.9)$$

Taking the exponential of both sides and solving for Te gives the following relation which is very useful for the determination of the mean fluid temperature at the tube exit.

$$T_e = T_s - (T_s - T_i) \exp(-hA_s/\dot{m} C_p) \qquad (3.10)$$

The temperature difference between the fluid and the surface decays exponentially in the flow direction, and the rate of decay depends on the magnitude of the exponent hAx /mCp, as shown in Fig 3.6

3.2 ONE-DIMENSIONAL FLOW THROUGH A 2D RECTANGULAR MICROCHANNEL

In this problem, as envisaged in Fig.3.7, the microchannel is viewed as two parallel plates placed one over the other extending into the z-direction and the flow is in the x-direction. It has been assumed that the z-directional dimension is equal to unity. The channel clearance length (b) is 0.1 mm or 100 μm. So far as the bulk properties of the fluids are concerned, 100 μm is still a scale governed by the classical laws of simple liquids and ideal gases under normal pressure. Therefore for ordinary liquids (fluids), the current micro fluidic device is subjected to the rules of classical fluid mechanics.

3.2.1 Assumptions in the analysis:

(1) All the liquid properties viz., density, viscosity, etc, are constant.

(2) The fluid is Newtonian in nature.

(3) The flow is laminar and the shear rates involved are small.

(4) The pressure gradients in all the directions, except in x-direction are zero.

(5) To simplify the problem, we consider the flow only in the x-direction and all the other directional velocities to be zero.

$$v_x = v_x(y) \quad v_y = v_z = 0 \quad p = p(x) \tag{3.11}$$

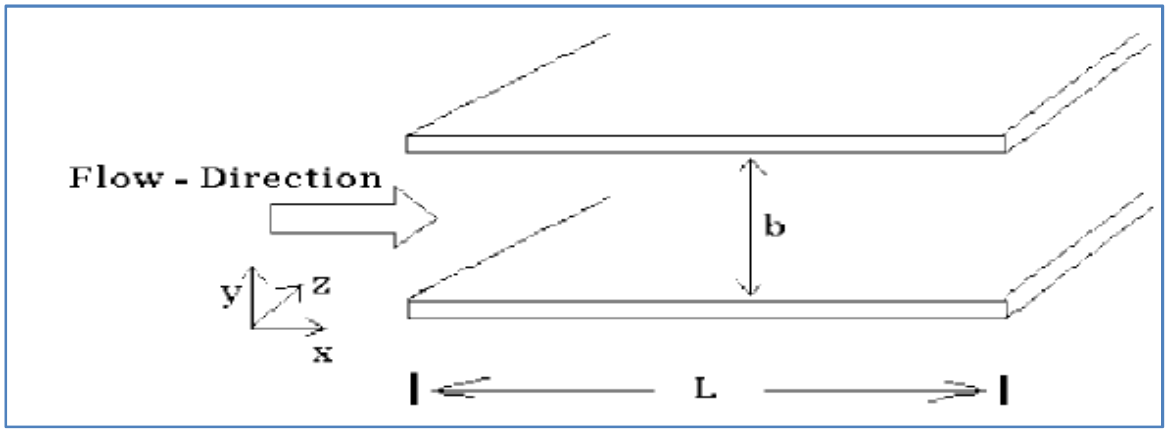

Fig 3.7 Microchannel for one-dimensional flow.

Classical fluid mechanics for macrochannels is based on no-slip boundary condition. At the walls of the microchannel, the velocity of the fluid is given by

$$V_x\big|_{wall} = L_s \left(\frac{\partial V_x}{\partial n} \right)\Bigg|_{wall} \qquad (3.12)$$

Where Ls is slip length and n is the normal coordinate pointing inward from the channel wall. Slip length can be referred to as extrapolation length; it is the distance from the wall at which the fluid is assumed to attain the normal parabolic velocity profile. The equations to be used to get the velocity profile are continuity and Navier–Stoke's equations along with the boundary condition Eqn (3.12) Velocity profile is given as

$$V_x = \frac{1}{2\mu}\frac{dp}{dx}\left[y^2 + (-b)(y_s + L_s) \right] \qquad (3.13)$$

Equation (3.13) is the starting equation for the analysis of one-dimensional velocity problem considered here, characterized by low-shear rates and negligible pressure gradients in directions other than the flow direction. By equating Eqn (3.13) to zero and solving the resulting quadratic equation, the value of y can be determined.The slip length can be assumed to be constant at any arbitrary point on the walls of the channel owing to its dependence on velocity gradient as given by the Eqn (3.14).

$$L_s = 0.192\left(\frac{dV_x}{dy} \right)^{0.46}_{wall} \qquad (3.14)$$

Average velocity is defined here as the ratio of flow rates along the x-axis direction of the channel to the cross-sectional area normal to the direction of flow, that is, the y–z plane. Mathematically, it can be expressed as:

$$\langle u \rangle = \frac{-b}{2\mu}\frac{dp}{dx}\left[L_s + \frac{b}{6}\right] = \frac{Q}{A} = \frac{Q}{b} \tag{3.15}$$

Where Q is the volumetric flow rate through the channel. This average velocity <u> is used to obtain the pressure distribution along the x-direction, also referred to as Hagen–Poiseuille's equation.

$$p_i - p_f = \frac{2\mu L Q}{b^2\left(\frac{b}{6} + L_s\right)} \tag{3.15}$$

It can be rearranged in the following form:

$$\Delta p = f_m \frac{\rho \langle u \rangle^2}{2}\left(\frac{L}{b}\right) \tag{3.16}$$

where G and <u> are the mass and average velocities, respectively, through the channel. The right-hand side of Eqn (3.17) has been expressed as a function of L/b and the kinetic head, and it can be conveniently expressed as

$$f_m = \frac{\left(\frac{4\mu}{G}\right)}{\left(L_s + \frac{b}{6}\right)} \tag{3.17}$$

Energy equation is given as

$$\rho C_P \left(u\frac{dT}{dx} + v\frac{dT}{dx}\right) = K\nabla^2 T \tag{3.19}$$

It is also evident from Eqns (3.17) and (3.18) that the pressure required to drive the fluid is lesser in microchannel than in comparison to macrochannel.

3.3 Numerical method

In this problem, a fictitious time derivative is introduced in the momentum equations. The pressure-correction based iterative SIMPLE mrthod has been used for solving the governing equations with the boundary conditions specified previously. The computational domain is divided into cartesian cells staggered grid arrangements (Fig. 3.8(a)) are used in which velocity components are stored at the midpoints of the cell sides to which they are normal. The pressure is stored at the center of the cell. A first-order implicit scheme is used for time derivative discretization. The u-momentum equation after integration over the u-control volume (Fig. 3.8(b)) becomes.

$$F_{\mathrm{e}}\phi_e - F_{\mathrm{w}}\phi_w + F_{\mathrm{n}}\phi_n - F_{\mathrm{s}}\phi_s = b \tag{3.20}$$

Where ϕ = u or ν and Fe is the nonlinear coefficient of φe . b contains the source terms, diffusive terms, and time derivative terms. The convective terms at any interface is estimated by a linear extrapolation of the φe values at two upwind neighbors; thus,

$$F_{\mathrm{e}}\phi_e = \left(\frac{3}{2}\phi_p - \frac{1}{2}\phi_w\right)\left|\left[F_e, 0\right]\right| - \left(\frac{3}{2}\phi_e - \frac{1}{2}\phi_{ee}\right)\left|\left[-F_e, 0\right]\right| \tag{3.21}$$

Where the symbol [|a, b|] represents the maximum of the two operands a and b. The diffusive terms at any interface is estimated by a linear interpolation between two grid point neighbors on either side of the interface. Thakur and Shy discussed the ‘upwind scheme’ in detail. The pressure link between continuity and momentum is accomplished by transforming the continuity equation into a Poisson equation for pressure. The Poisson equation implements a pressure correction for a divergent velocity field.

A single iteration consists of the following sequential steps:

(1) An implicit calculation of the u, v momentum equations is performed through a block elimination method.

(2) The Poisson equation for pressure correction is solved using a Gauss–Seidel iteration method with the successive under relaxation technique. In this case, the under-relaxation factor is chosen as 0.7

(3) The velocity field at each cell is updated using the pressure correction

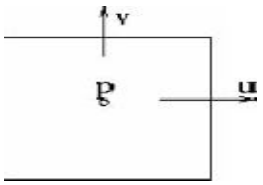

Fig.3.8(a)

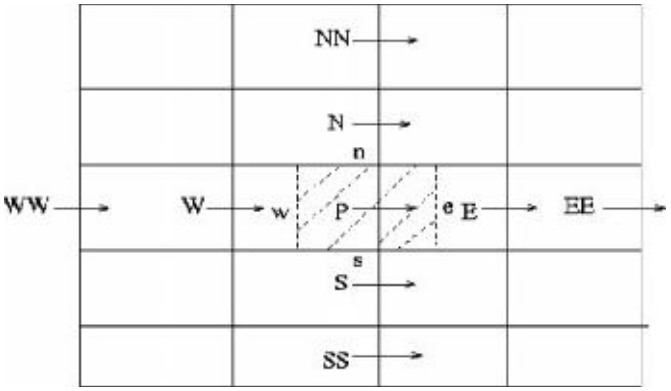

Fig.3.8(b) Schematic of 3.8(a) p-control volume and 3.8(b) u-control volume.

(4) Convergence criteria is employed of the form

$$\left| \phi_{i,j}^{n+1} - \phi_{i,j}^{n} \right| < \varepsilon \tag{3.22}$$

Here, i and j denotes the cell index, n is the time level, φ is u or v. The value of ε is assumed to be 10−4. Flow is assumed to start impulsively from rest.To facilitate the convergence of the solution for a given higher Reynolds number, the converged solution of a case with smaller Re is used as the initial guess.

3.4 Grid consideration and algorithm testing

A non-uniform grid distribution is incorporated in the computational domain. Figure 4 shows the grid distribution inside the channel and at the entrance of the channel (up to x = 10). In order to resolve the gradients in a better way, the grid is finer near the channel walls and at the inlet. To check the grid sensitivity, we performed computations for four set of grids namely,1000 × 150, 1500 × 100, and 1000 × 100; with the first and second number being the number of mesh points in the x- and y-direction, respectively. The maximum distance of the first grid point from each wall and from the entrance of the channel are 0.01b and 0.005b, for the coarse and fine grids, respectively. We find that the change in solution for different grid size occurs on the third decimal place. We find that 1000 × 100 grids are optimum.

Chapter 4

CFD ANALYSIS

4.1 WHAT IS COMPUTATIONAL FLUID DYNAMICS (CFD)?

Computational Fluid Dynamics (CFD) is a computer-based numerical tool used to study the fluid flow, heat transfer behavior and also its associated phenomena such as chemical reaction. A set of mathematical model equations are first developed following conservation laws. These equations are then solved using a computer program in order to obtain the flow variables throughout the computational domain. Examples of CFD applications in the chemical process industry include drying, combustion, separation, heat exchange, mass transfer, pipeline flow, reaction, mixing, multiphase systems and material processing. Validation of CFD models is often required to assess the accuracy of the computational model. This assessment can assist in the development of reliable CFD models. Validation is achieved by comparing CFD results with available experimental, theoretical, or analytical data. Validated models become established as reliable, while those which fail the validation test need to be modified and revalidated.

4.2 FLUENT AND GAMBIT

FLUENT is the general name for the collection of computational fluid dynamics (CFD) programs sold by FLUENT, Inc. FLUENT is a computational fluid dynamics (CFD) solver that provides a wide array of advanced physical models for fluid flow and heat transfer applications including multiphase flow. FLUENT has a preprocessor called GAMBIT. FLUENT is the CFD solver which can handle both structured grids, i.e. rectangular grids with clearly defined node indices, and unstructured grids. Unstructured grids are generally of triangular nature, but can also be rectangular. In 3-D problems, unstructured grids can consist of tetrahedral (pyramid shape), rectangular boxes, prisms, etc.

GAMBIT is the program used to generate the grid or mesh for the CFD solver. Most commands in Gambit require the user to select an object (a vertex, en edge, etc.). To select an object, hold down the Shift key on the keyboard, and click on the object with the left mouse button. In most cases, an alternate way to select is provided by a List window, which allows the user to click on object(s) from the Available column, and transfer them to the Picked column. This is especially useful when an operation is to be done on many objects at the same time. In cases where more than one object can be selected by the same click (for example two faces which share an edge), the first Shift click may pick the "wrong" one. In such a case, Shift click with the middle mouse button until the desired one is selected.

4.3 MODELLING IN CFD

Regardless of the type of problem following are the steps involved in CFD

1. Preprocessing
2. Solution stage
3. Post processing

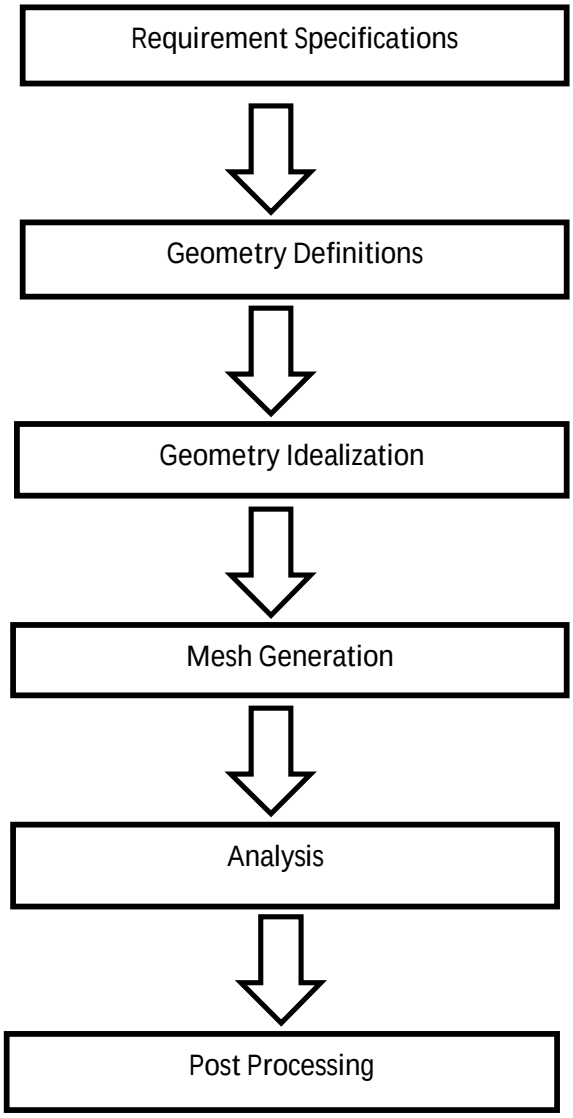

Fig 4.1 Flow chart for CFD

4.3.1 Geometry

The geometry is created in the Gambit 2.2.30.Following are the steps involved.

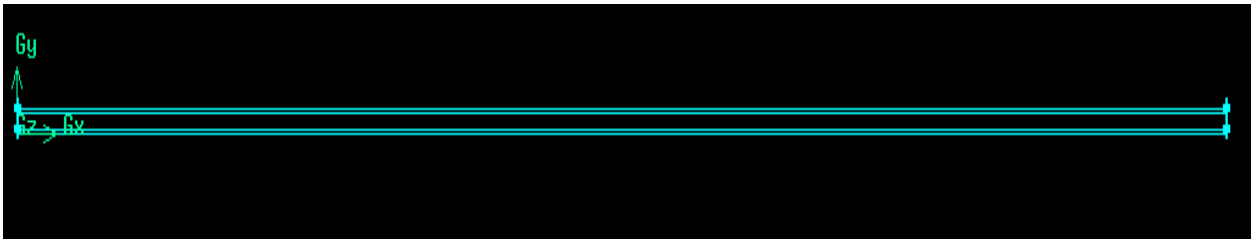

Fig 4.2 Geometry of 2D micro channel

Key points:

Select to **create face**

Face → rectangular face

In the box write H=0.1&W=10.It will create a rectangular face with height 0.1 and length=10.

4.3.2 Meshing

The geometry is created in the Gambit 2.2.30.Following are the steps involved.

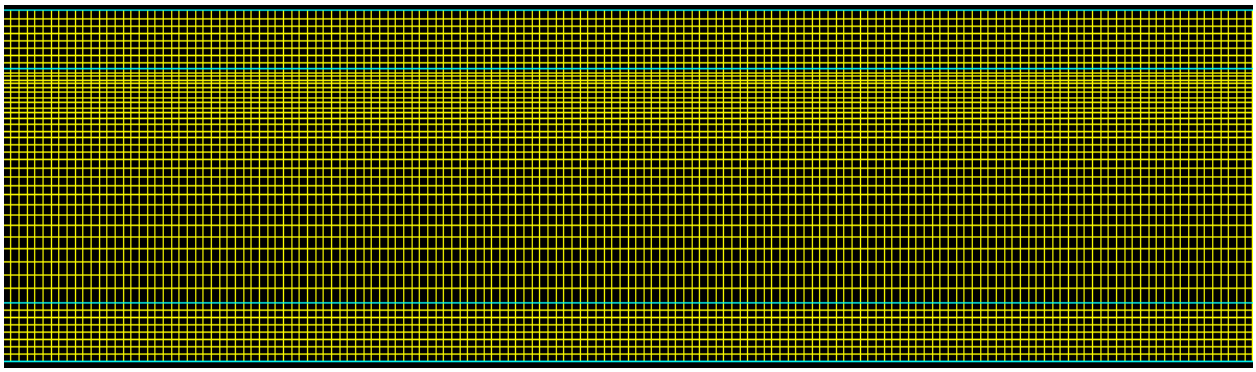

Fig 4.3 Meshing of 2D micro channel

Key points

Select **meshing**

Meshing→ Edge meshing→ Select two edges→ Click apply

In the box for interval count write 1000 for the left and right edges.

Meshing→ Edge meshing→ Select two edges→ Click apply

In the box for interval count write 100 for the top and bottom edges.

Face meshing→ select face→ Click OK

Specify **boundary types**

Select edge→ specify boundary conditions→ Click OK

Select the boundary types. In the box write name of the boundary condition.

Specify **Zone types**

Select face →specify zone types→ Click OK

In the box write the name of face (solid/fluid zone).

Export the mesh file (.MSH) to Ansys13 Fluent

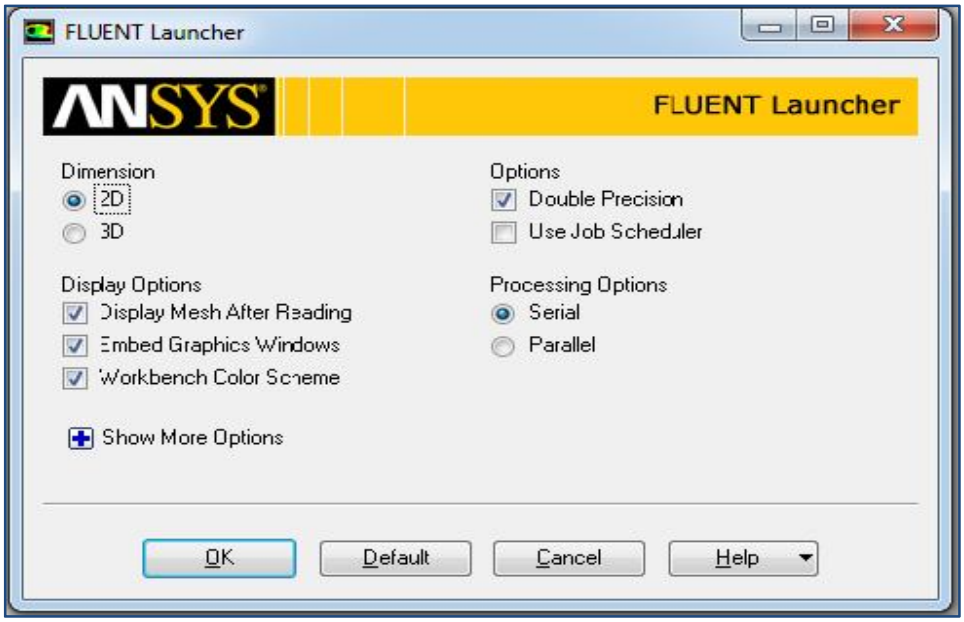

Fig 4.4 Fluent launcher in ANSYS

4.3.3 Problem set up

Check Grid

Check the **scale, quality** and **size** of the mesh.

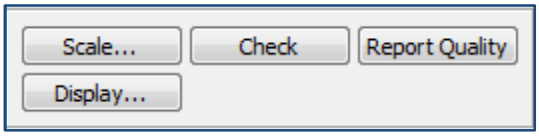

Fig 4.5 Display of grid properties

Models

Specify the model to be used, **Laminar viscous**.

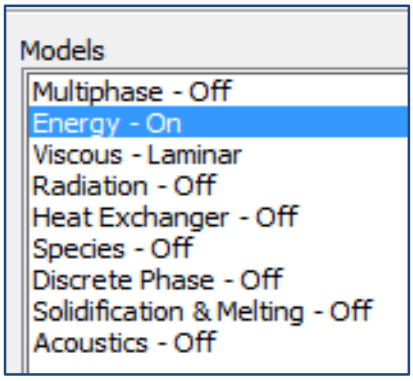

Fig 4.6 Various model used in FLUENT

Material

Specify the material for different zone

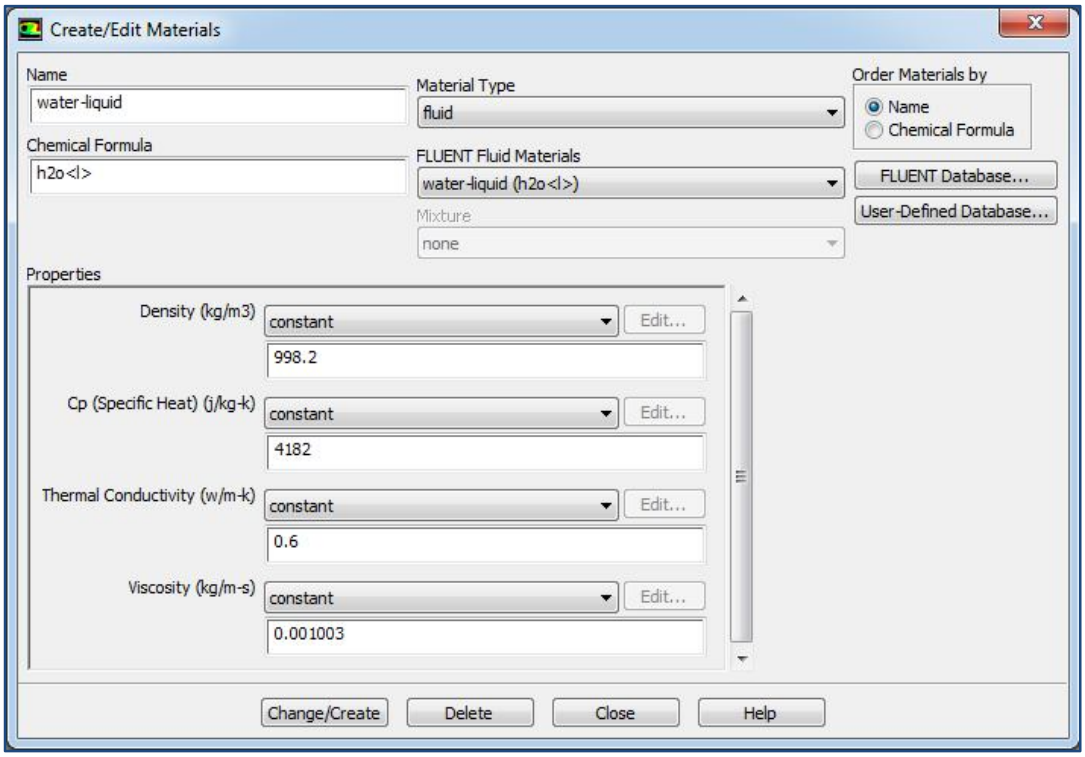

Fig 4.7 Material properties

Boundary condition and **cell zone condition.**

Specify the boundary condition and cell zone condition for different edges and faces.

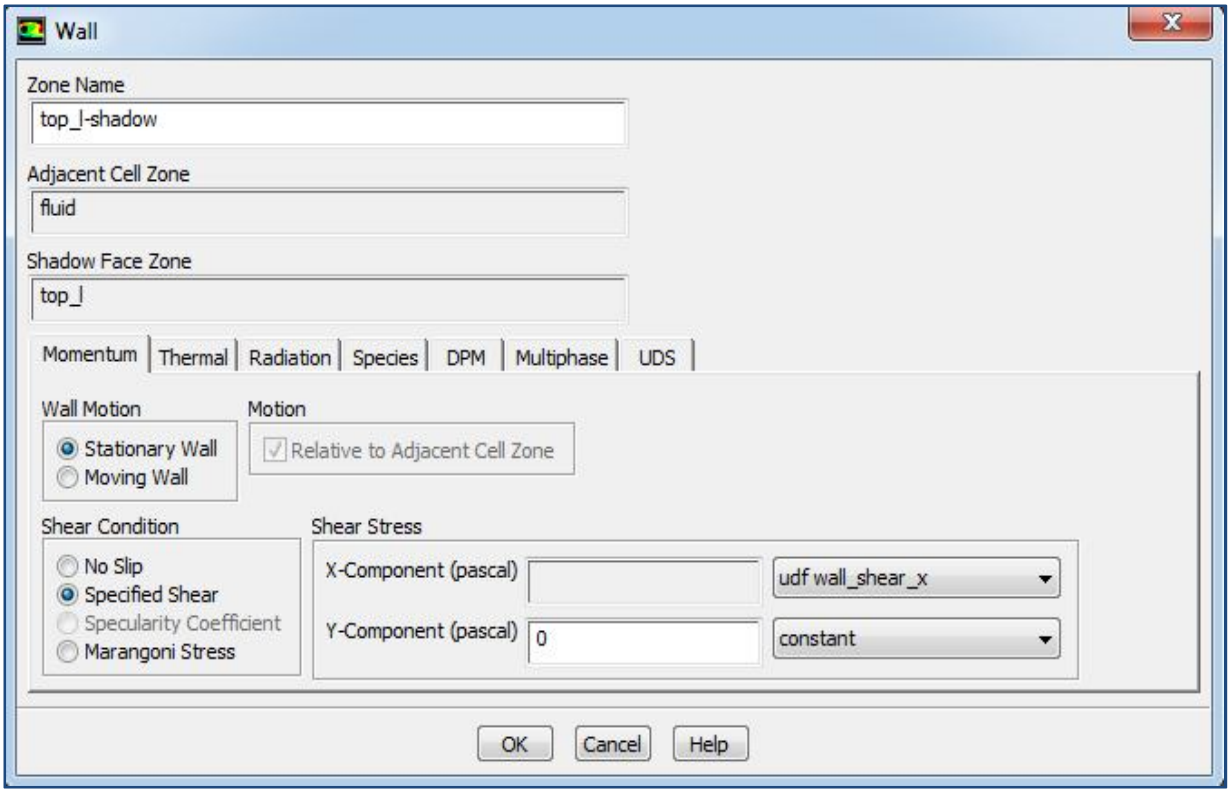

Fig 4.8 Boundary condition

Solution

Solution method and solution control

Specify the scheme and gradient for solution and under-relaxation factor

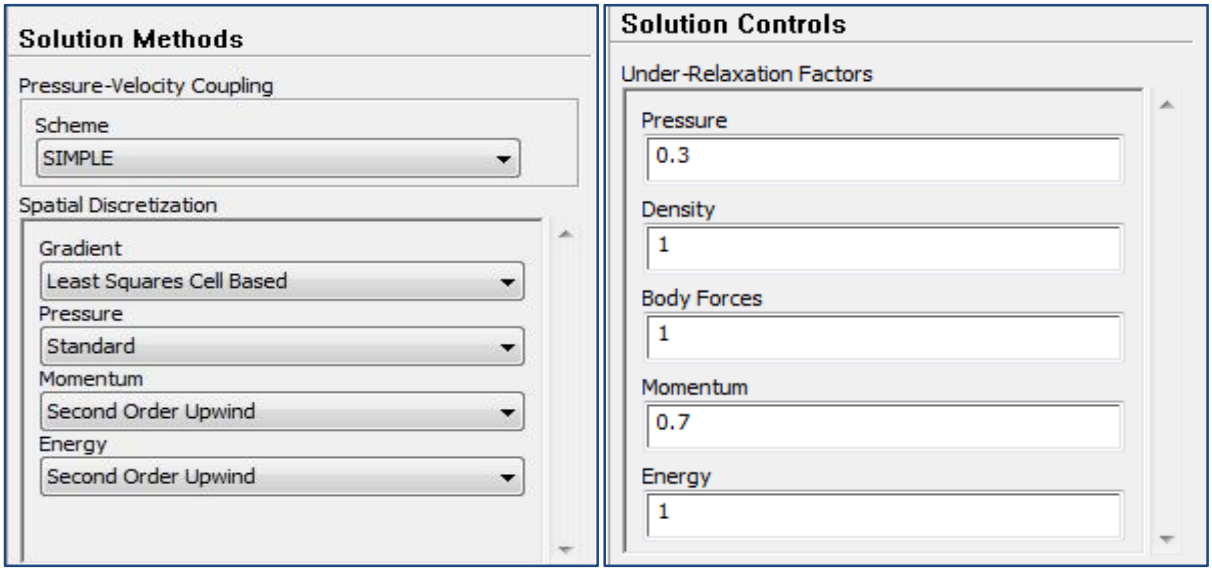

Fig 4.9 Solution control and solution method

Solution Initialization

Select the standard initialization and compute from inlet.

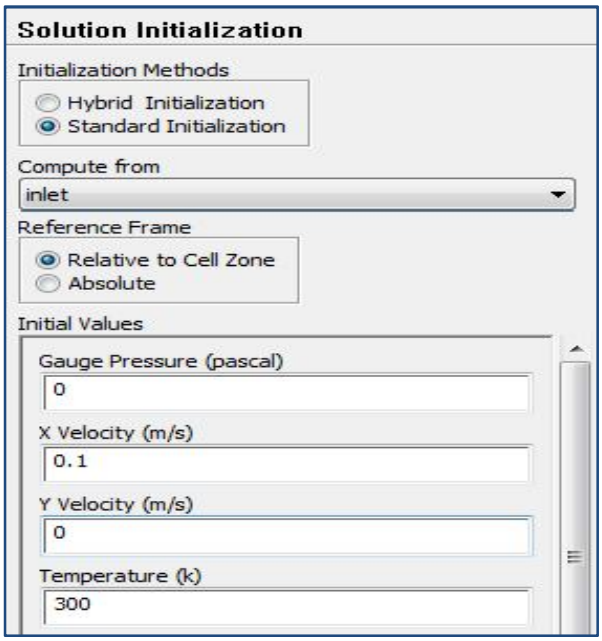

Fig 4.10Solution initialization

Results

Use the post-processor to display and plot the result.

Chapter 5

RESULT AND DISCUSSION

5.1 COMPUTATIONAL FLUID DYNAMICS MODEL

In this the single phase models is used for solving the respective category problems. This model will calculate one transport equation for the momentum and one for continuity for each phase, and then energy equations are solved to study the thermal behavior of the system. The theory for this model is taken from the ANSYS Fluent 13.

5.1.1 Mass Conservation Equation

The equation for conservation of mass, or continuity equation, can be written as follows:

$$\left(\frac{\partial u}{\partial x} + \frac{\partial v}{\partial y} \right) = 0 \tag{5.1}$$

Equation (5.1) is the mass conservation equation for incompressible flow.

5.1.2 Momentum Conservation Equation

$$\rho\left(u\frac{\partial u}{\partial x} + v\frac{\partial u}{\partial y} \right) = -\frac{\partial p}{\partial x} + \mu\left(\frac{\partial^2 u}{\partial x^2} + \frac{\partial^2 u}{\partial y^2} \right) \tag{5.2}$$

Equation (5.2) is the u-momentum equation for steady incompressible flow.

5.1.3 Energy Conservation Equation

$$\rho C_p\left(u\frac{\partial T}{\partial x} + v\frac{\partial T}{\partial y} \right) = k\left(\frac{\partial^2 T}{\partial x^2} + \frac{\partial^2 T}{\partial y^2} \right) \tag{5.3}$$

Equation (5.3) is the energy equation for steady incompressible flow.

5.2 SIMULATION OF SINGLE PHASE FLUID FLOW IN MACROPIPE

5.2.1 Physical Model

The fig 5.1 shows the physical model used in Ansys13 Fluent. The boundary condition was specified as velocity inlet and pressure outlet at the inlet and outlet. The model was analyzed for both constant temperature and constant heat flux at the upper wall. The local Nusselt and heat transfer coefficient was obtained for both the condition.

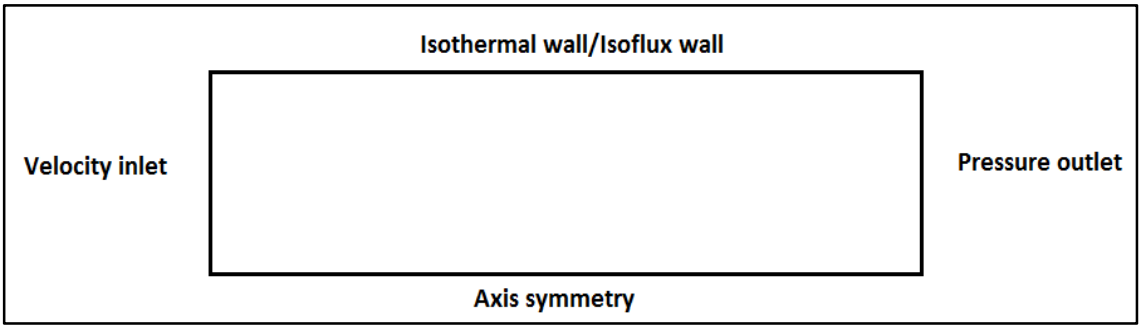

Fig 5.1 Physical model used in Ansys13 Fluent.

The velocity profile was obtained for inlet velocity of 0.25m/s and temperature profile was obtained for 350K.The velocity profile and temperature profile remains parabolic in the fully developed region.

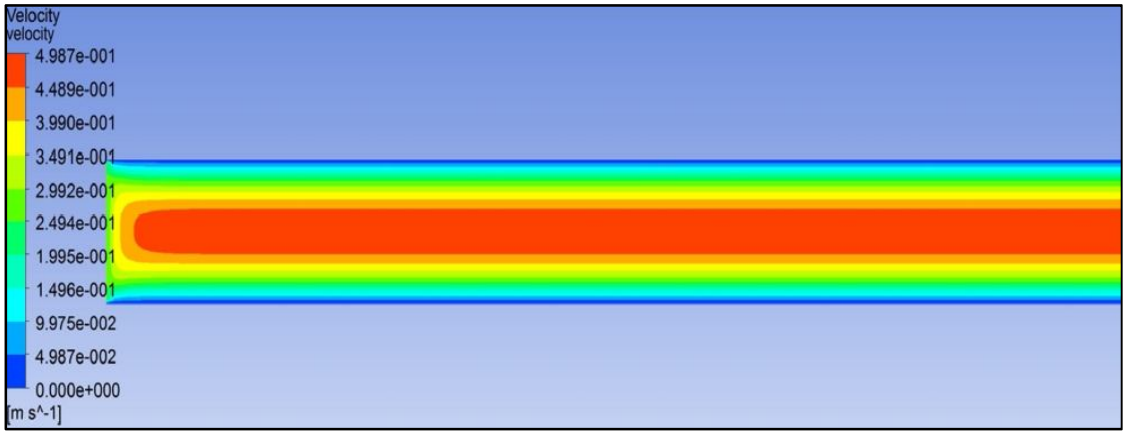

Fig 5.2 Velocity profile for macropipe with constant heat flux condition

Consider a fluid entering a circular tube at a uniform velocity. As in external flow, the fluid particles in the layer in contact with the surface of the tube will come to a complete stop. This

layer will also cause the fluid particles in the adjacent layers to slow down gradually as a result of friction. To make up for this velocity reduction, the velocity of the fluid at the midsection of the tube will have to increase to keep the mass flow rate through the tube constant. As a result, a velocity boundary layer develops along the tube.

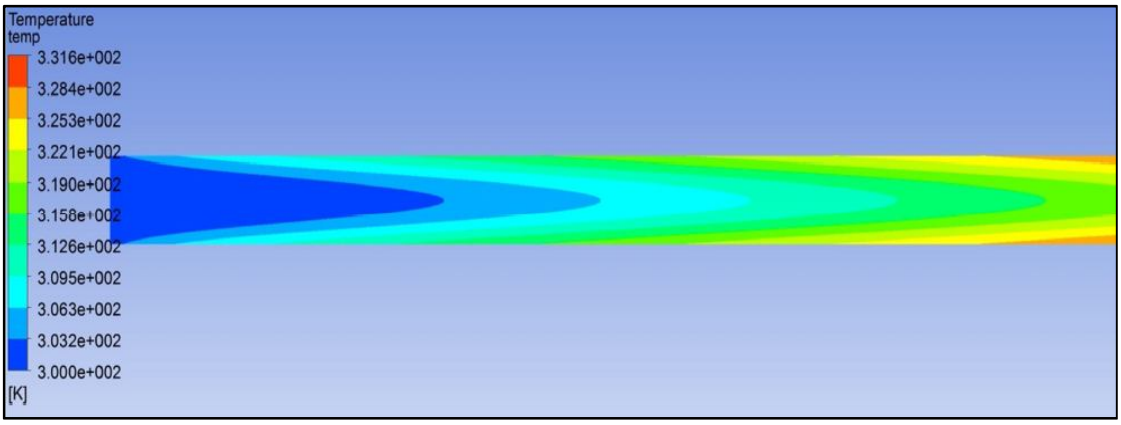

Fig 5.3 Temperature profile for constant heat flux condition

The thickness of this boundary layer increases in the flow direction until the boundary layer reaches the tube center and thus fills entire tube, as shown in Figure 5.2.The region from the tube inlet to the point at which the boundary layer merges at the centerline is called the **hydrodynamic entrance region,** and the length of this region is called the **hydrodynamic entry length** L_h. Flow in the entrance region is called hydrodynamically developing flow since this is the region where the velocity profile develops. The region beyond the entrance region in which the velocity profile is fully developed and remains unchanged is called the **hydrodynamically fully developed region.** The velocity profile in the fully developed region is parabolic in laminar flow .The temperature profile is for the heated fluid .The fluid enters with inlet temperature of 300K and reaches a maximum temperature of 331.6K. The temperature and velocity profile is one dimensional in the developed region.

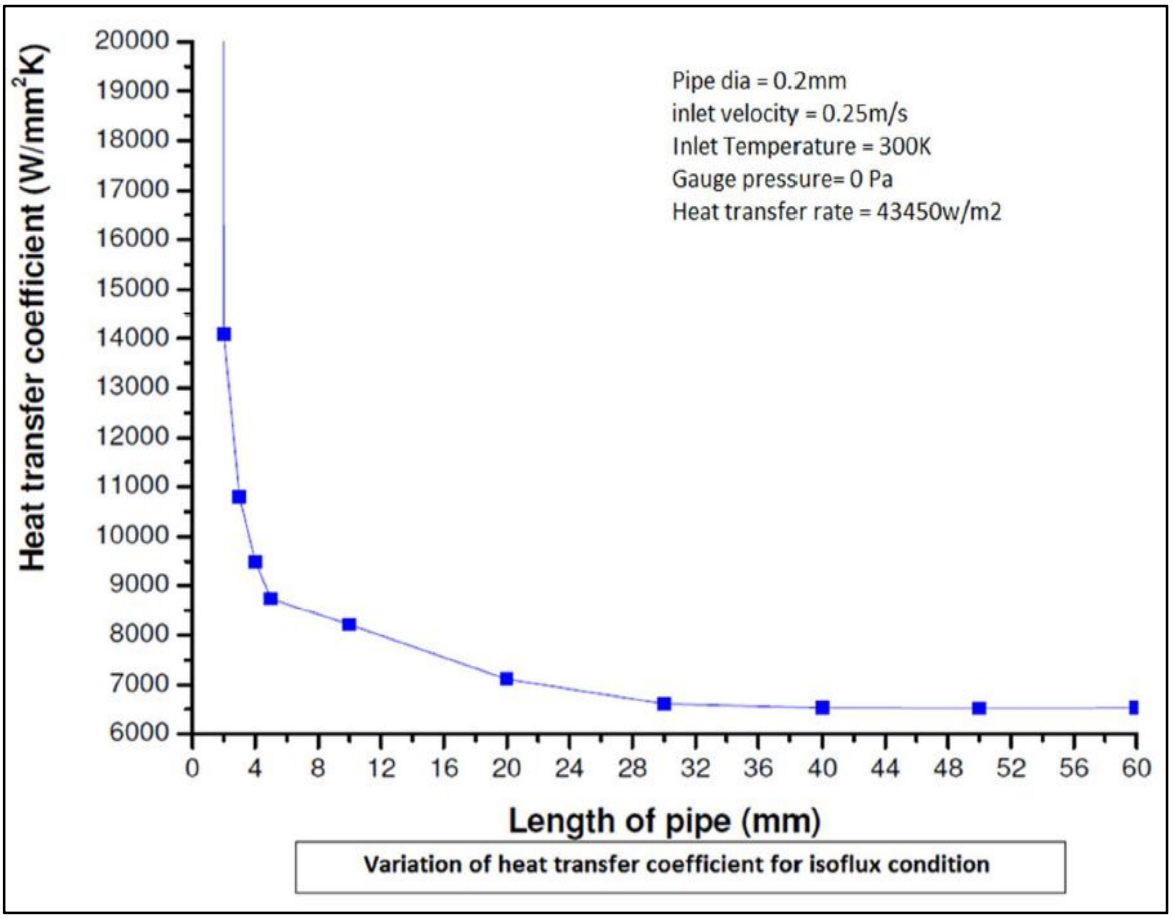

Fig 5.4 Variation of heat transfer coefficient as a function of length of pipe for isoflux condition.

The heat transfer coefficient initially start from a higher value and decreases uniformly up to 30mm length of the pipe in the entrance region and remain constant in the fully developed region.

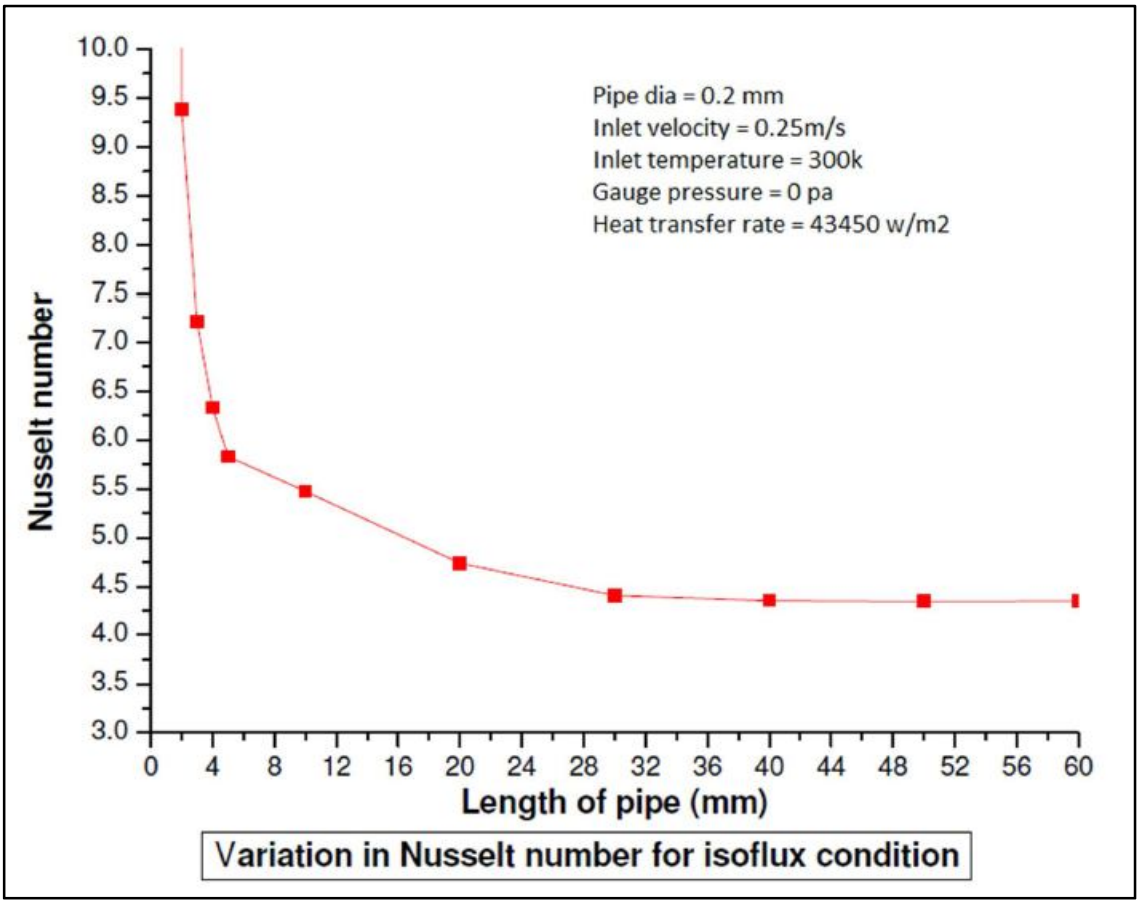

Fig 5.5 Variation of Nusselt number as a function of length of pipe for isoflux condition.

The Nusselt number starts initially from a higher value in the entrance region and start decreasing uniformly up to 30mm length of the pipe .In the fully developed region the Nusselt number remains constant, which is **4.36**. The mean temperature was found to vary linearly along the length of pipe.

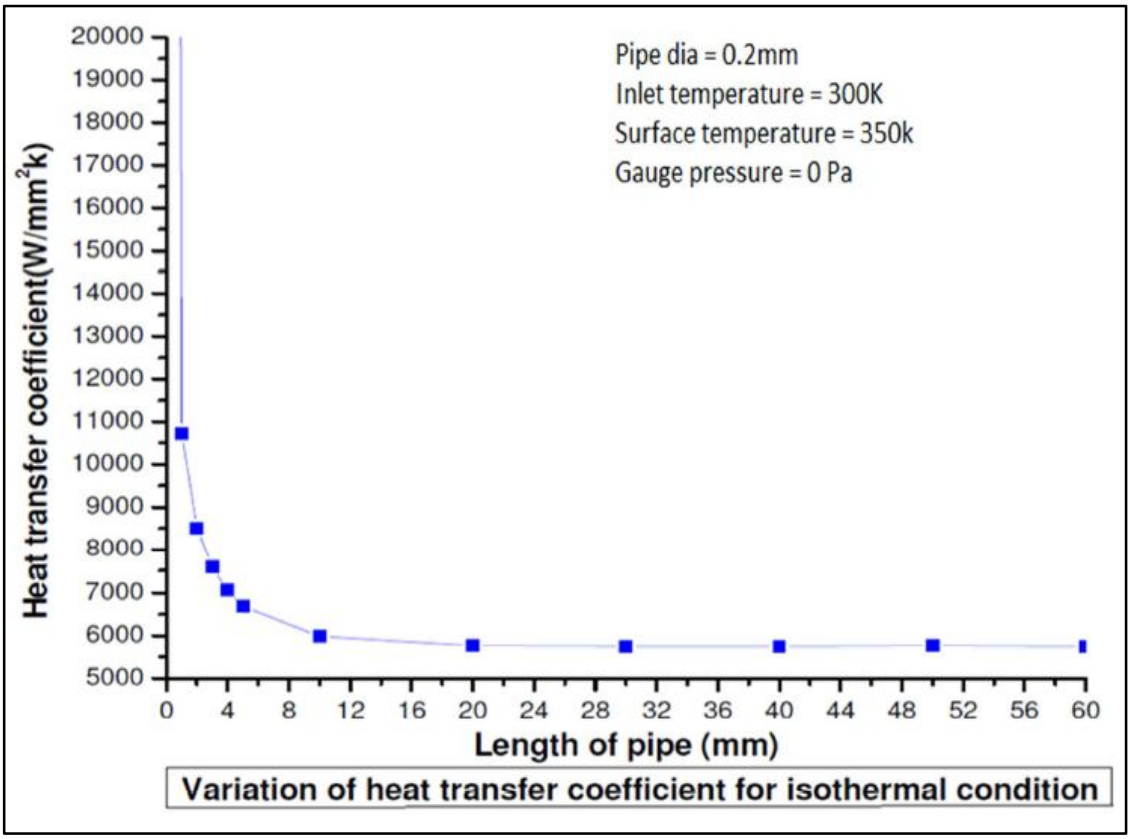

Fig 5.6 Variation of heat transfer coefficient as a function of length of pipe for isothermal condition

The heat transfer coefficient initially start from a higher value and decreases uniformly up to 30mm length of the pipe in the entrance region and remain constant in the fully developed region. The mean temperature was found to vary exponentially along the length of pipe

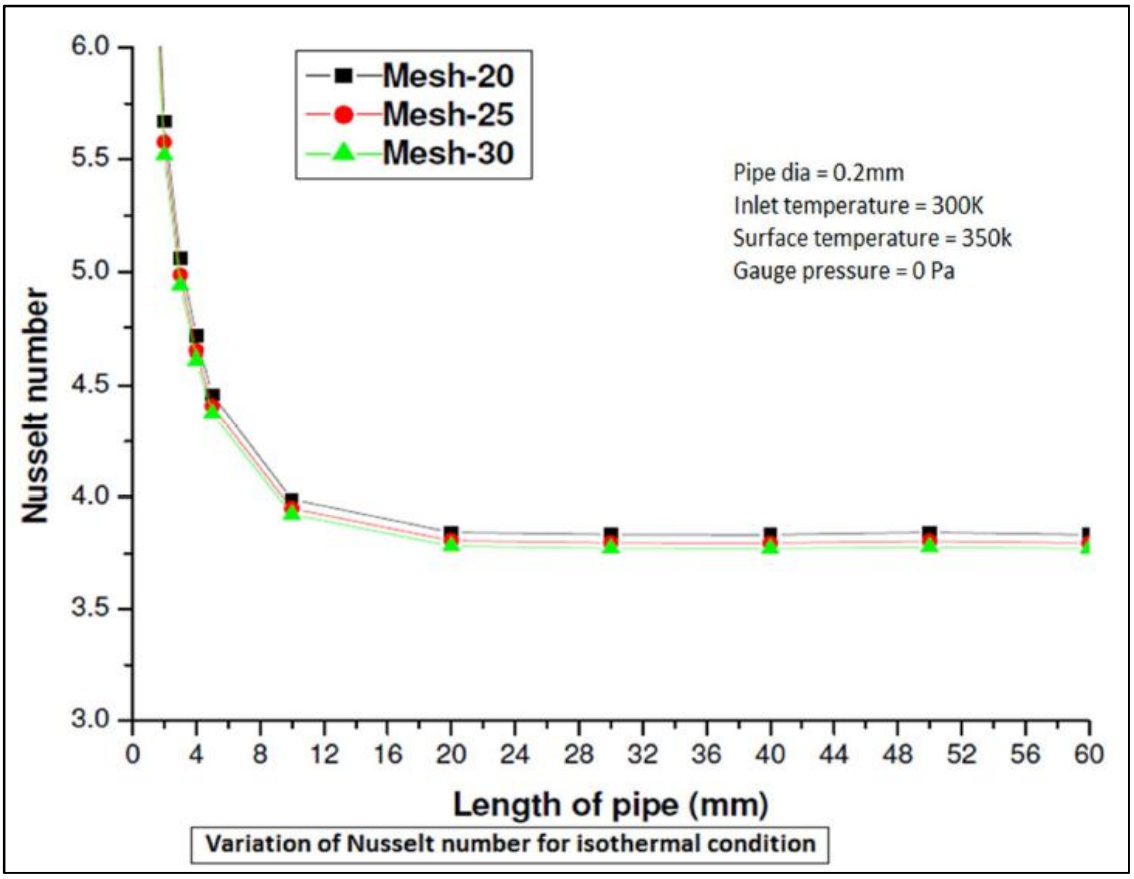

Fig 5.7 Variation of Nusselt number on of as a function of length of pipe for isothermal condition

The Nusselt number starts initially from a higher value in the entrance region and start decreasing uniformly up to 30mm length of the pipe .In the fully developed region the Nusselt number remains constant which is **3.63**. The Nusselt number obtained are in good approximation with the analytical value.

5.3 1D FLOW THROUGH 2D RECTANGULAR MICROCHANNEL

5.3.1Physical Model

The fig 5.8 shows the physical model of a 2D rectangular microchannel. The length of the channel is 10cm and width is 0.1mm.The inlet and outlet condition was specified as velocity inlet and pressure outlet.

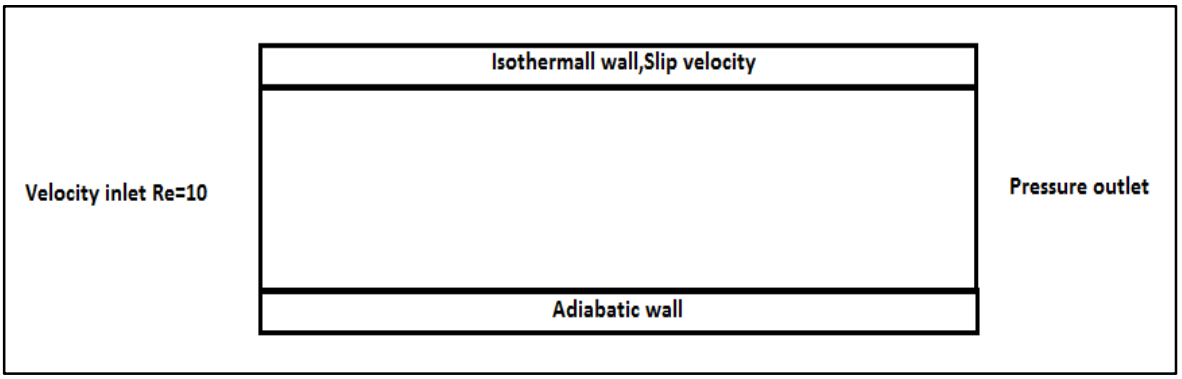

Fig 5.8 Physical model of a 2D rectangular mic rochannel.

The upper wall was given a constant temperature of 365K and the lower wall was specified as adiabatic wall. The slip condition was specified at the upper wall in terms of UDF (User defined function), the UDF was defined in order to implement the slip velocity at the wall. The inlet velocity was specified with Reynolds number Re=10. The inlet velocity was varied to compare the velocity profiles at different Reynolds number.

5.3.2 FLOW SIMULATION AND DISCUSSION

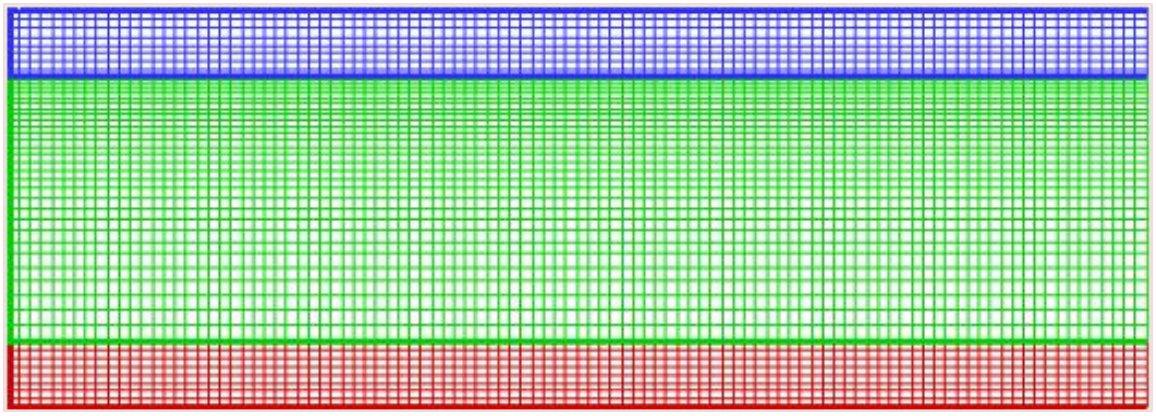

Fig 5.9 Mesh of the geometry obtained from Techplot

The fig 5.9 shows the mesh generation in the channel. The mesh was created using Gambit 2.2.30 software. The mesh was created finer near to upper wall. At the wall, the slip velocity boundary condition was specified in terms of the shear stress at the wall by writing small UDF which necessarily expresses the shear stress in terms of pressure gradient. The velocity profile get flattened near the wall, it increases near the entrance region and remains nearly constant in the fully developed region as shown in the fig 5.10

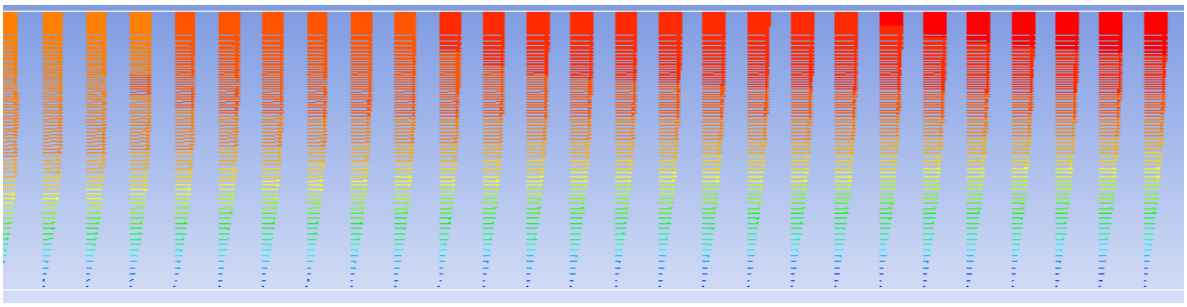

Fig 5.10 Velocity vector for slip flow

Flattening in the velocity profile is a phenomenon that has been found on the basis of one-dimensional flow problem. The velocity starts from zero at the bottom wall and reaches maximum at the upper wall and remain constant in the fully developed region.

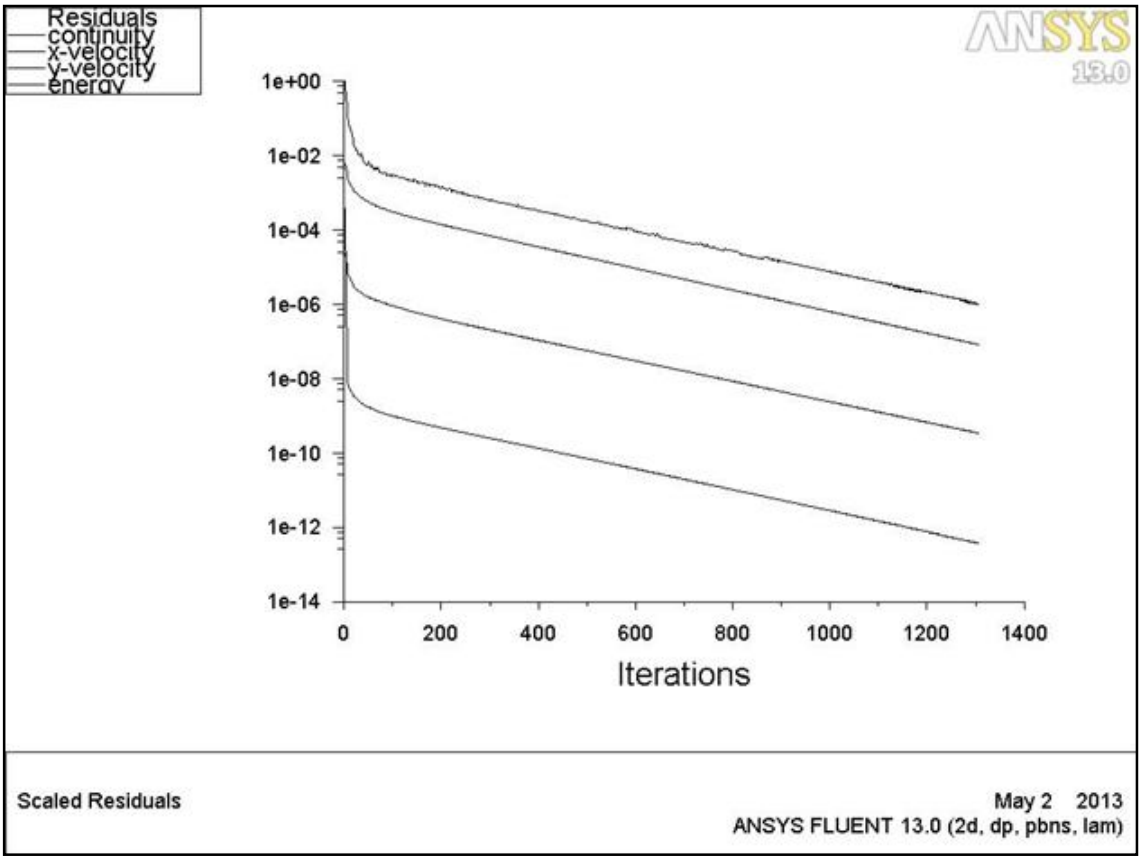

Fig 5.11 Residual Plot in FLUENT

The above figure shows the residual plot. The solution is converged at 1303 number of iteration. The residual limit was set to 10^{-6} for continuity and 10^{-7}energy equation. The residual for continuity fluctuates little bit at the start but becomes asymptote as the iteration progressed. The iteration was saved 100 per iterations.

5.3.3 FLUID FLOW ANALYSIS

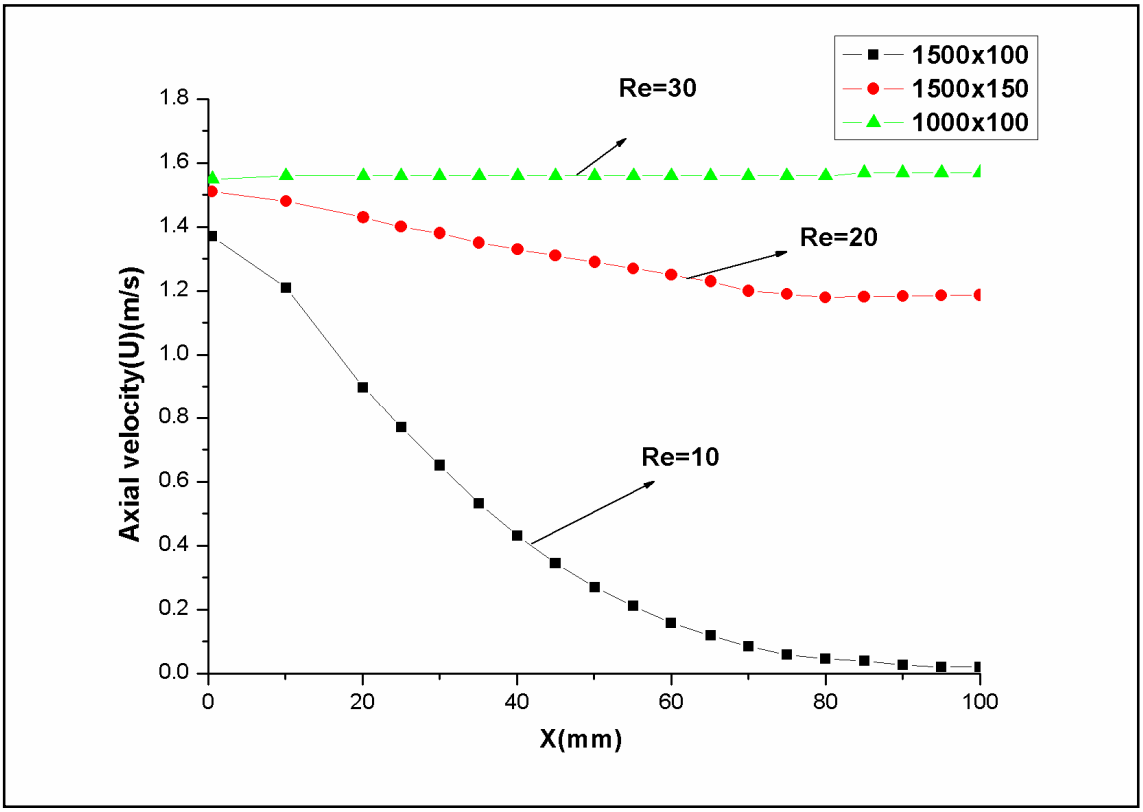

Fig 5.12 Axial velocity (u) along the centerline of the channel for different Re = 10, 20 &30

The effect of Reynolds number on flattening in velocity profile is shown in fig.5.12.The values obtained is in close resemblance to that calculated theoretically. Other methods for shear stress evaluation involve defining a line/rake at the required surface and hence obtaining the wall fluxes (in XY plot option). The shear stress are very small due to slip condition at the wall, it is of the order of 10^{-3}.

The wall shear stress obtained by the above methods are summarized as follows:

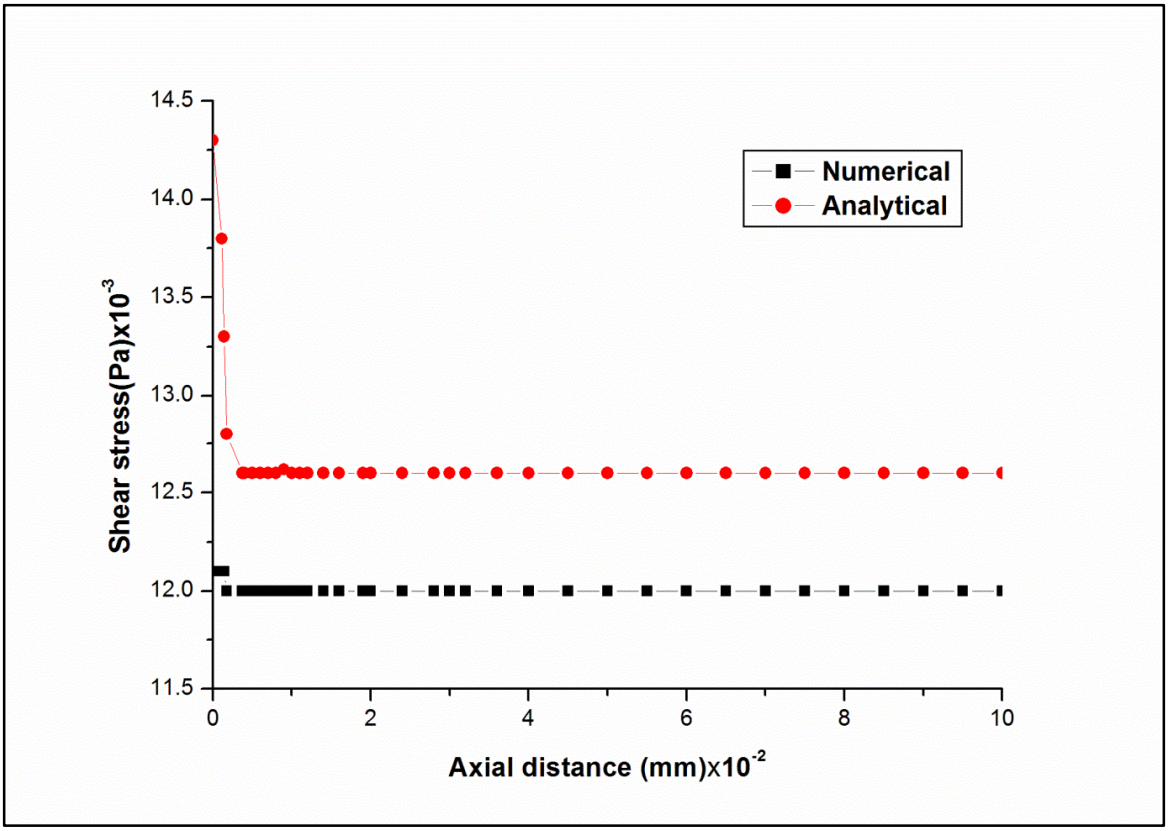

Fig 5.13 Variation of shear stress along the length of channel

The velocity contour obtained from Techplot is shown below. The velocity is zero at the bottom wall throughout the length of channel, but at the upper wall it remains constant in the fully developed remain region. It is flat at the upper wall and zero at the lower wall due to no-slip condition.

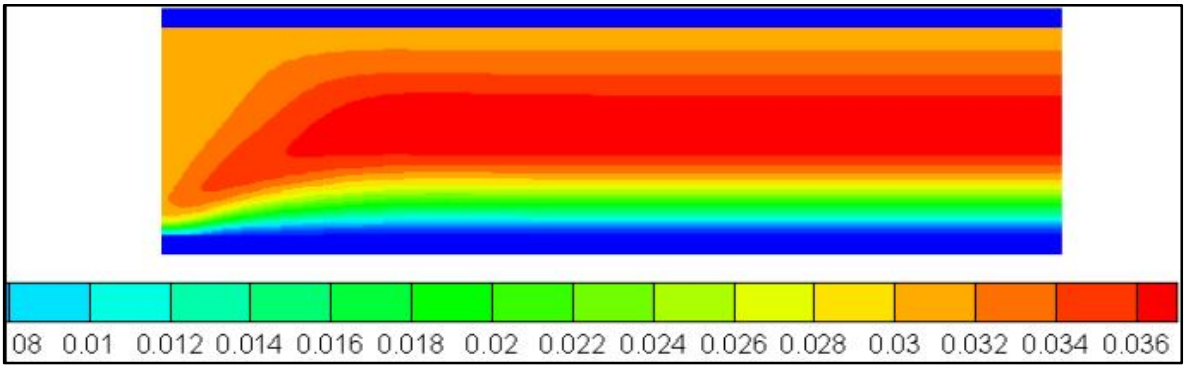

Fig 5.14 Velocity contour

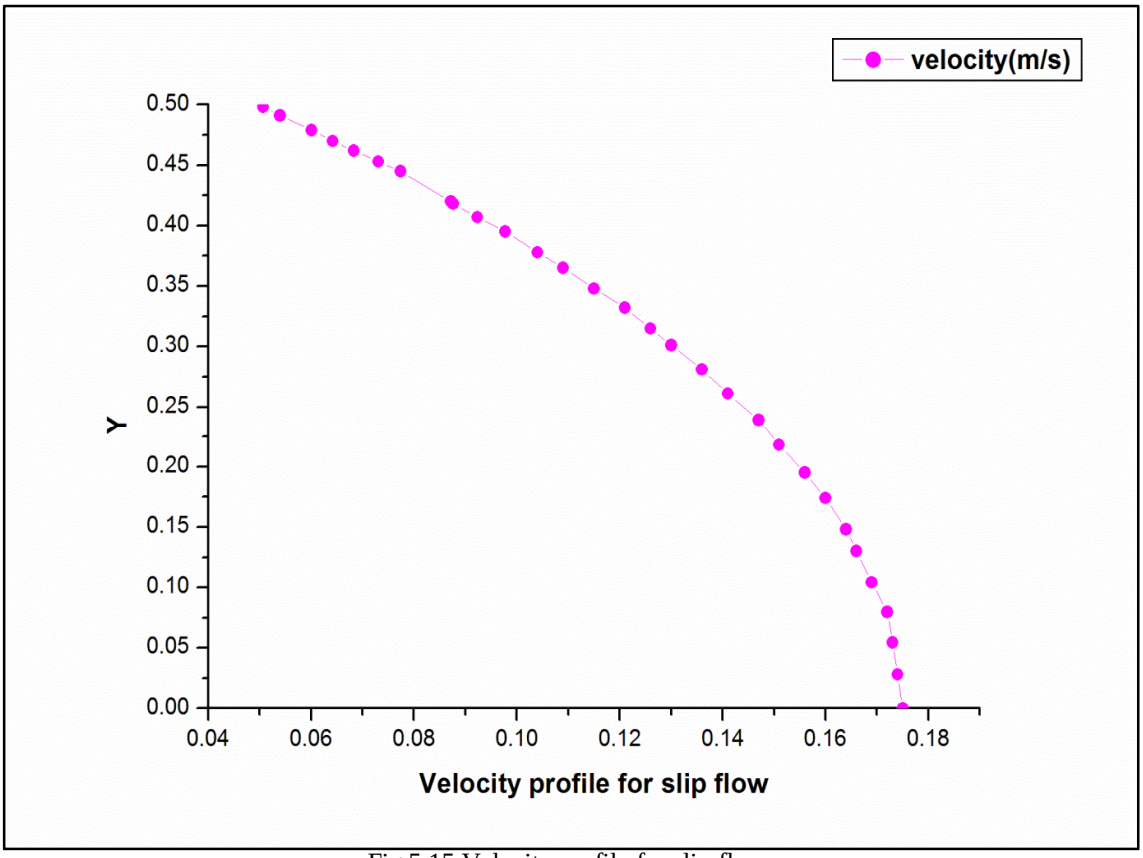

Fig 5.15 Velocity profile for slip flow

The velocity profile when the slip depends upon the shear stress is shown in the fig 5.15.The shear stress at the wall is specified in terms of UDF at the wall which essentially expresses the shear stress in terms of pressure gradient. The flow is assumed to be fully developed the pressure gradient is linear along the length of the channel, and there is no flow in the vertical direction.

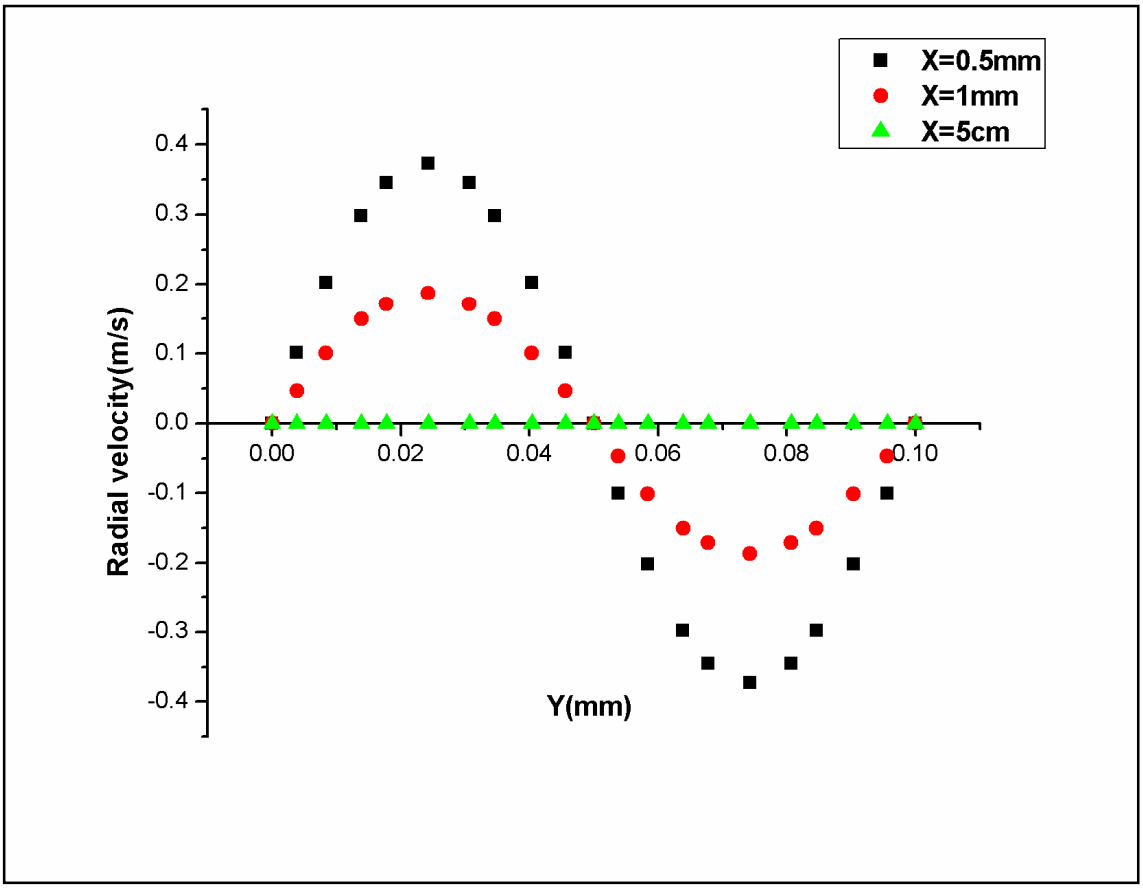

Fig 5.16 Radial velocity profile along radial direction through the channel.

Fig.5.16 shows the radial velocity profile, along the radial direction at different x and Re = 10 at the entrance of the channel, velocity in the radial direction is very small in comparison with that in the axial direction. It is evident from Fig5.16 that after a certain value of x, at which flow has been fully developed, the change in radial velocity component is very negligible; it behaves as a one-dimensional flow.

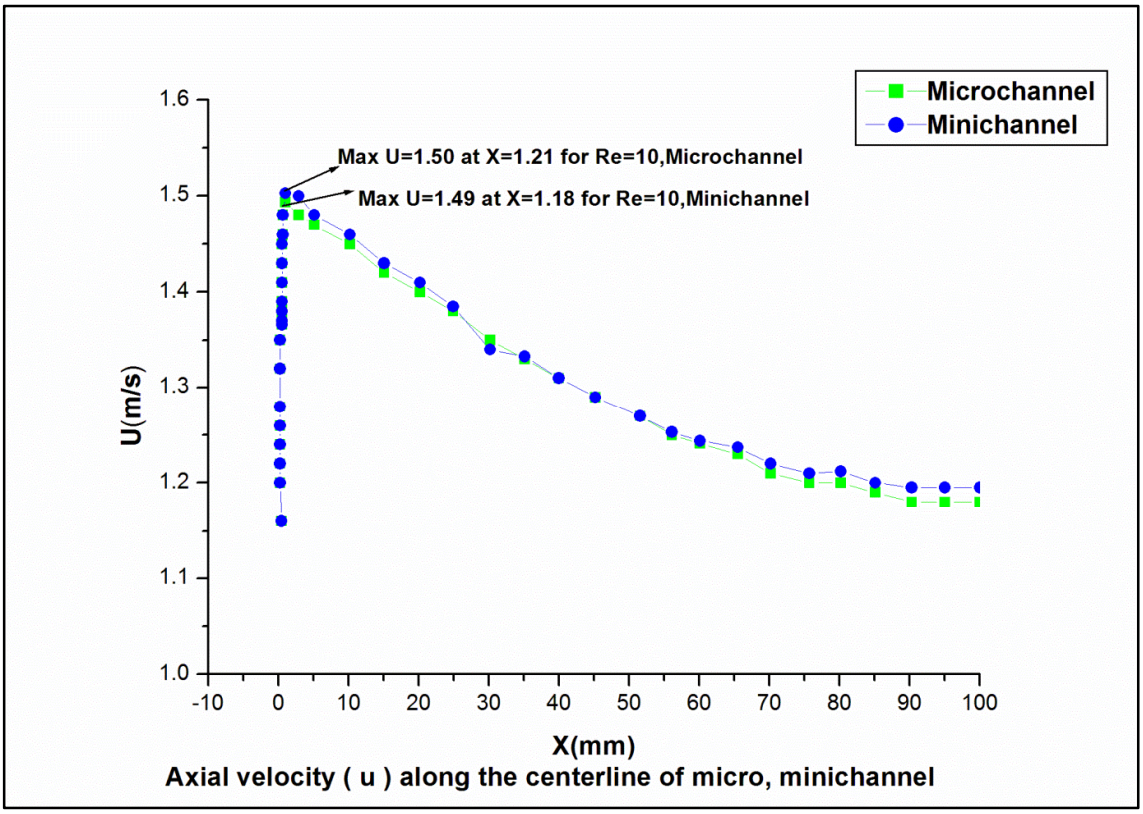

Fig 5.17 Variation of axial velocity along the centerline of micro, minichannel.

The effect of Reynolds number on flattening of longitudinal velocity profile for a mini-channel (b=1 mm, L=10 cm, with no-slip boundary condition) and a proper macrochannel (b=10 cm, L=1 m, with no-slip boundary condition) has been compared in Fig.5.17. In a proper microchannel for Re = 10 the non-dimensional axial velocity develops to a value of 1.503 at x =1.21, then the flattening begins in the velocity profile. Whereas for mini channel, non-dimensional axial velocity develops to a value of 1.4935 at x =1.179 for Re =10, then the flattening begins in the velocity profile. After the length of x =1.179, the mini-channel behaves like a proper microchannel. Actually, it is the slip effect that delays the formation of fully developed velocity profile in proper microchannel with slip boundary condition. For the proper macrochannel the velocity profile could not be developed for same inflow rate within

this channel span because $Re_{macro} = \frac{b_{macro}}{b_{micro}} Re_{micro}$ for the same inflow rate. It can be concluded that the flattening in the velocity profile in microchannel owes to the small scale of the dimensions of the channels involved.

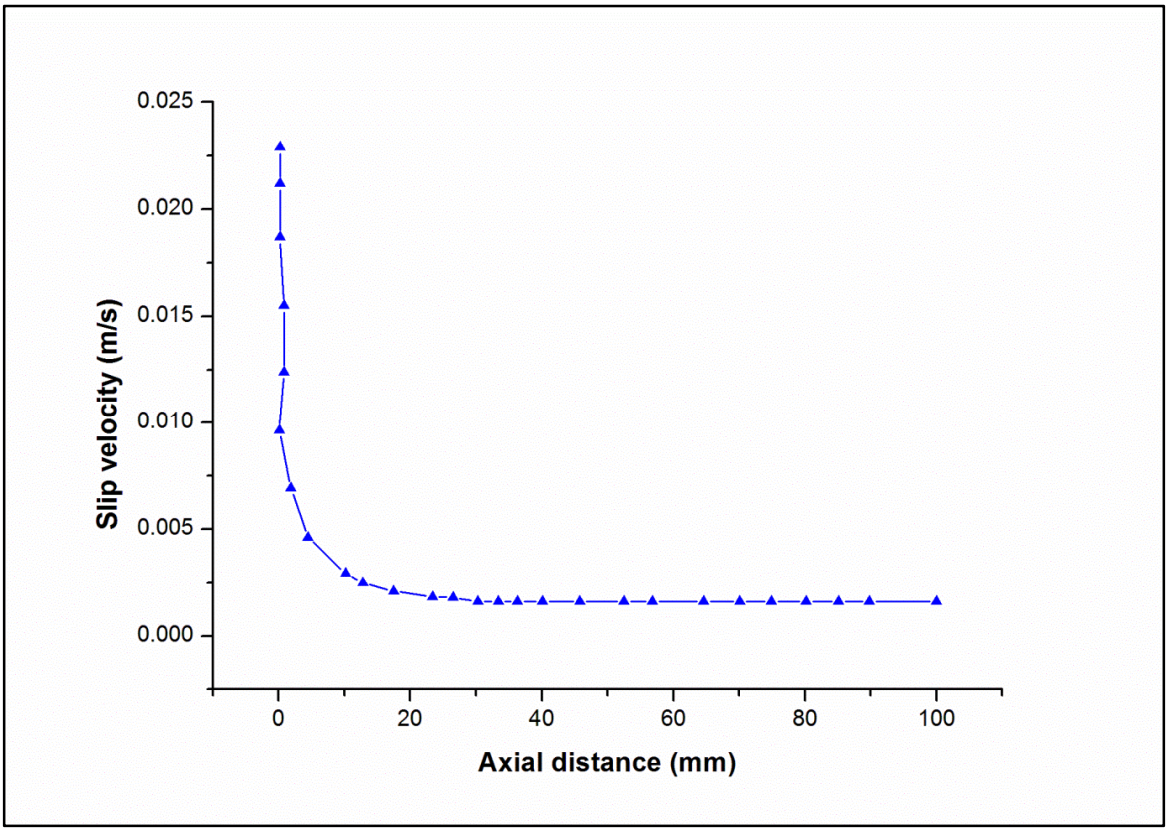

Fig 5.18 Slip velocity as a function of the axial distance

The slip velocity is independent of the radial component of the velocity. The slip velocity is a decreasing function of the axial dimension and has been found on simulation as shown in Fig.5.18. At x = 10 and onwards, the slip velocity is negligible; hence, the channel onwards behaving as a minichannel, that is, channel with micro dimension but with no-slip condition. This is also evident from Fig. that the axial dimensional dependency of velocity (u), beside its

radial dimensional dependency, is to be considered within this short span of channel length for microchannels in practice.

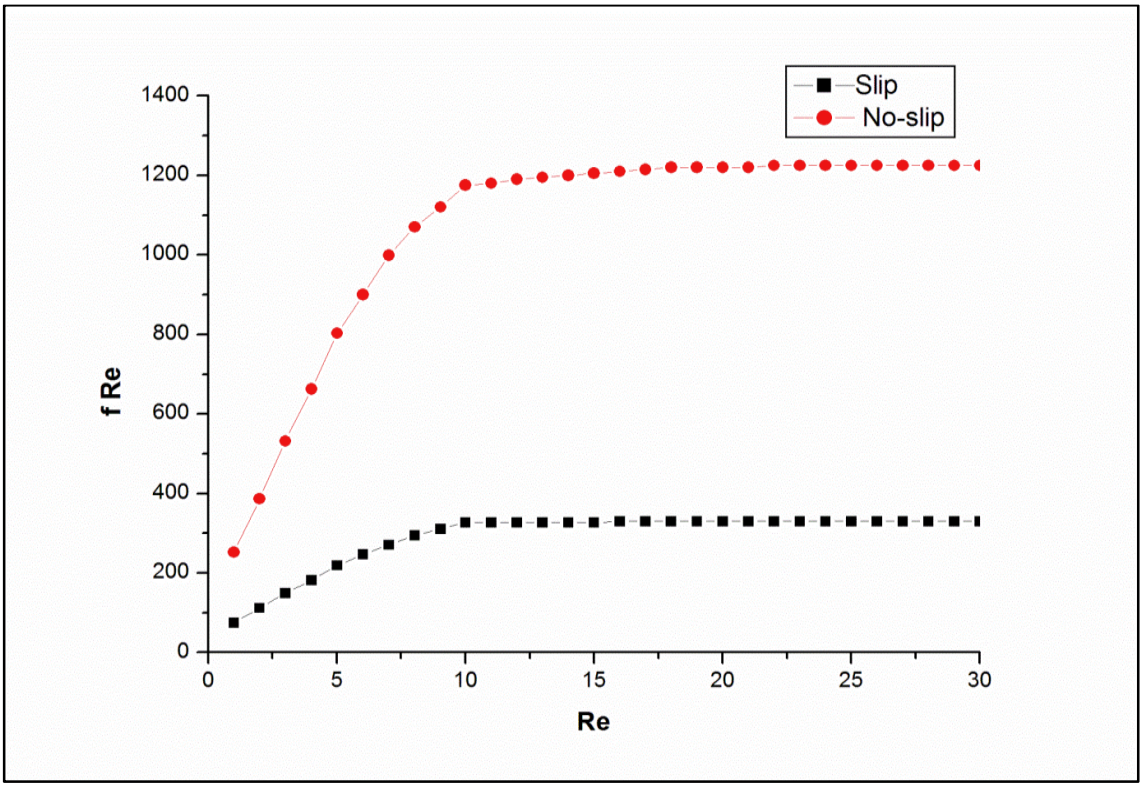

Fig 5.19 Variation of fRe as function Reynolds number of both for slip and no-slip conditions.

Fig. 5.19 shows the simulated values of fRe (f being the local friction factor & Re being the local Reynolds number) both for slip and no-slip conditions. The f. Re value for a slip value is much lower than a no-slip flow. This is due to the fact that slip effect reduces the wall friction significantly, hence, there is a reduction in driving pressure.

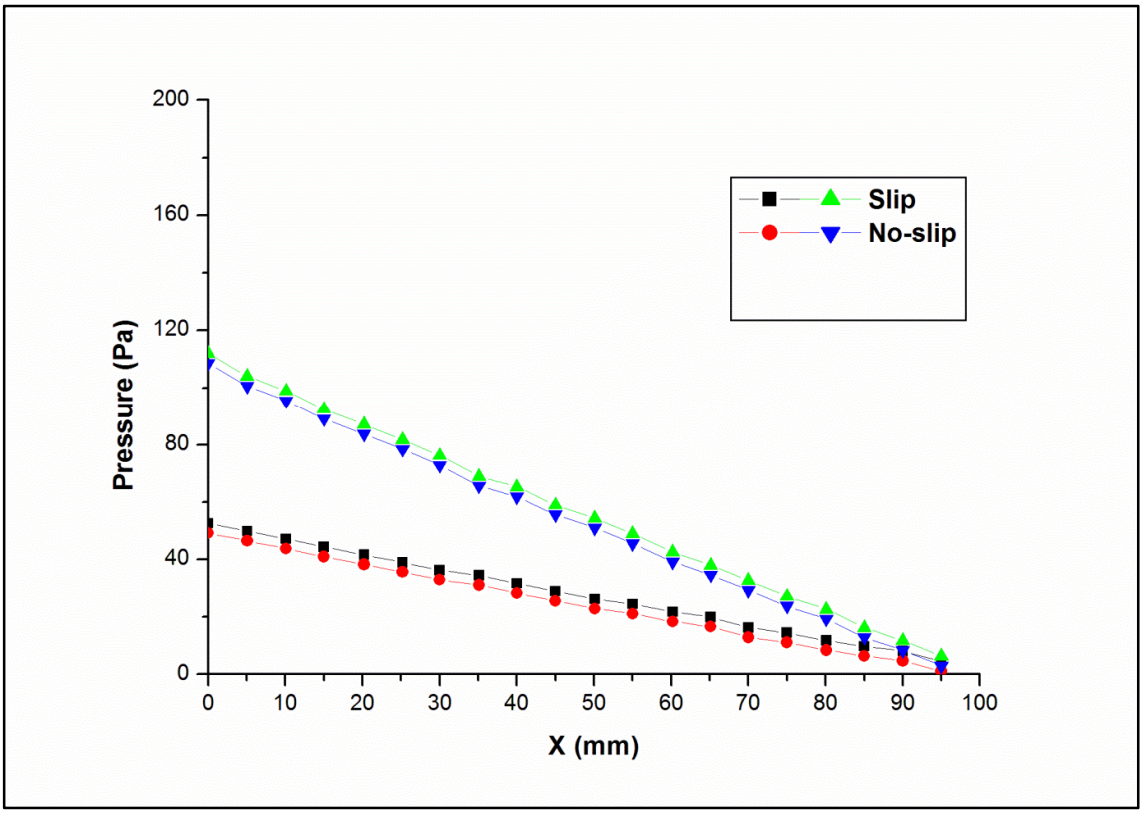

Fig 5.20 Pressure variation in microchannel

The possibility of compression in liquid flowing through a microchannel is further strengthened from fig.5.20, which shows that the nonlinearity in pressure distribution with decreasing Reynolds number for a microchannel flow may cause compressibility effect. This nonlinearity in pressure distribution, hence the corresponding compressibility effect, as discussed by Chen[12], in the numerical simulation for flow of gases through microchannels is much more pronounced than in comparison with the liquid micro flows.The curvature in pressure distribution curve for the slip flow is less than in no-slip flow because of reduced friction in the case of slip flow.

5.3.4 HEAT TRANSFER ANALYSIS

The effect of length of channel and pipe on the Nusselt number and also the variation of mean temperature and non-dimensional Nusselt number as a function of non-dimensional number x/b for different values of Reynolds number has been studied and explained briefly as below.

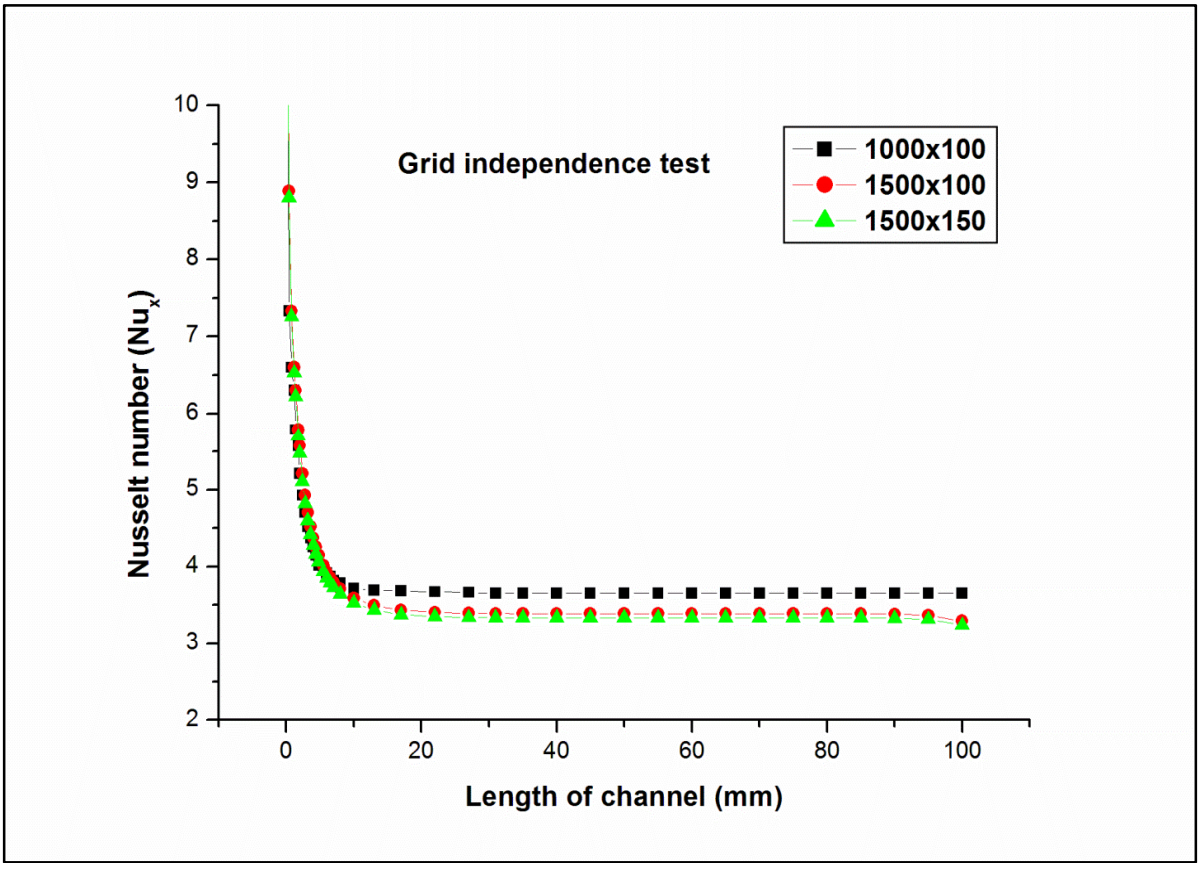

Fig 5.21 Variation of Nusselt number as function of length of channel

A grid independence test was carried as shown in the fig 5.21.The mesh points with 1000x100 give the optimum value. The Nusselt increases with slip flow, the increase in the value is approximately 19%.The effect of axial conduction is considered in calculating the Nusselt number. For isothermal condition the Nusselt increases but for constant heat flux it decreases. The effect of slip is to increase the heat transfer coefficient.

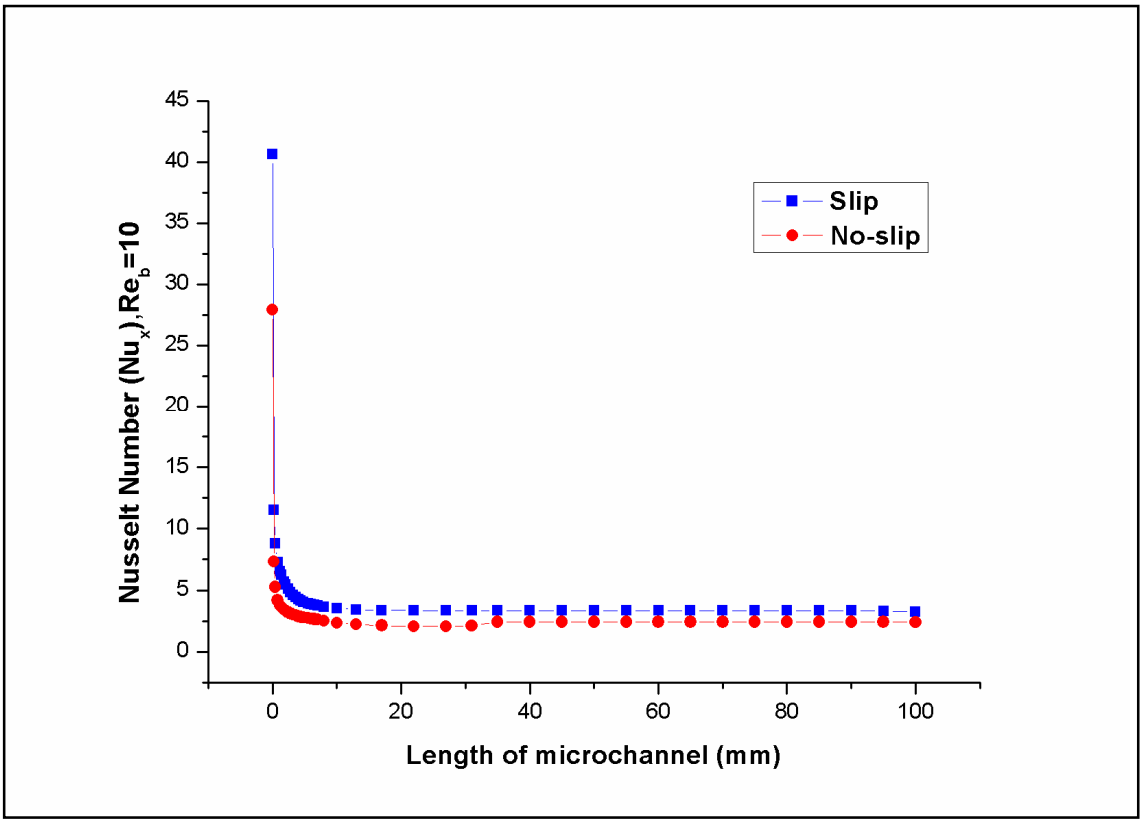

Fig 5.22 Variation of Nusselt number as function of length of pipe for slip and no-slip

The fig 5.22 shows the local Nusselt number variation along the length of pipe for slip and no-slip condition, the Nusselt number for the slip condition increases as compared to the no-slip condition. The average value of Nusselt number obtained was 3.66 with slip condition, while that of no-slip condition obtained was less.

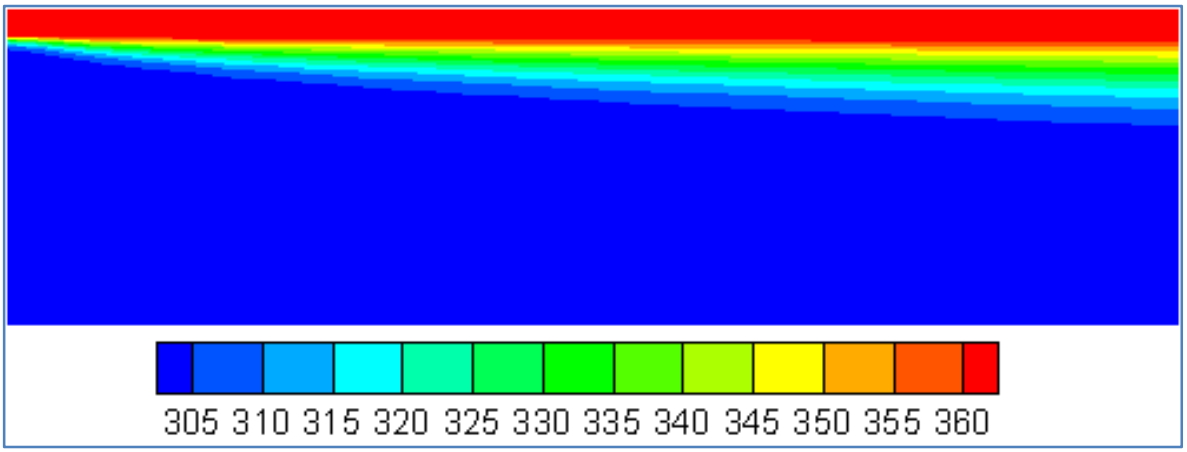

Fig 5.23 Temperature contour of micro channel.

Fig 5.23 shows the temperature profile inside the microchannel. The wall temperature was given 365K, which remained constant throughout the length of microchannel for isothermal condition. The fluid inlet temperature increase from 300K at the inlet to a maximum temperature of 360K at the outlet. The dimensionless temperature profile remains constant in the fully developed region.

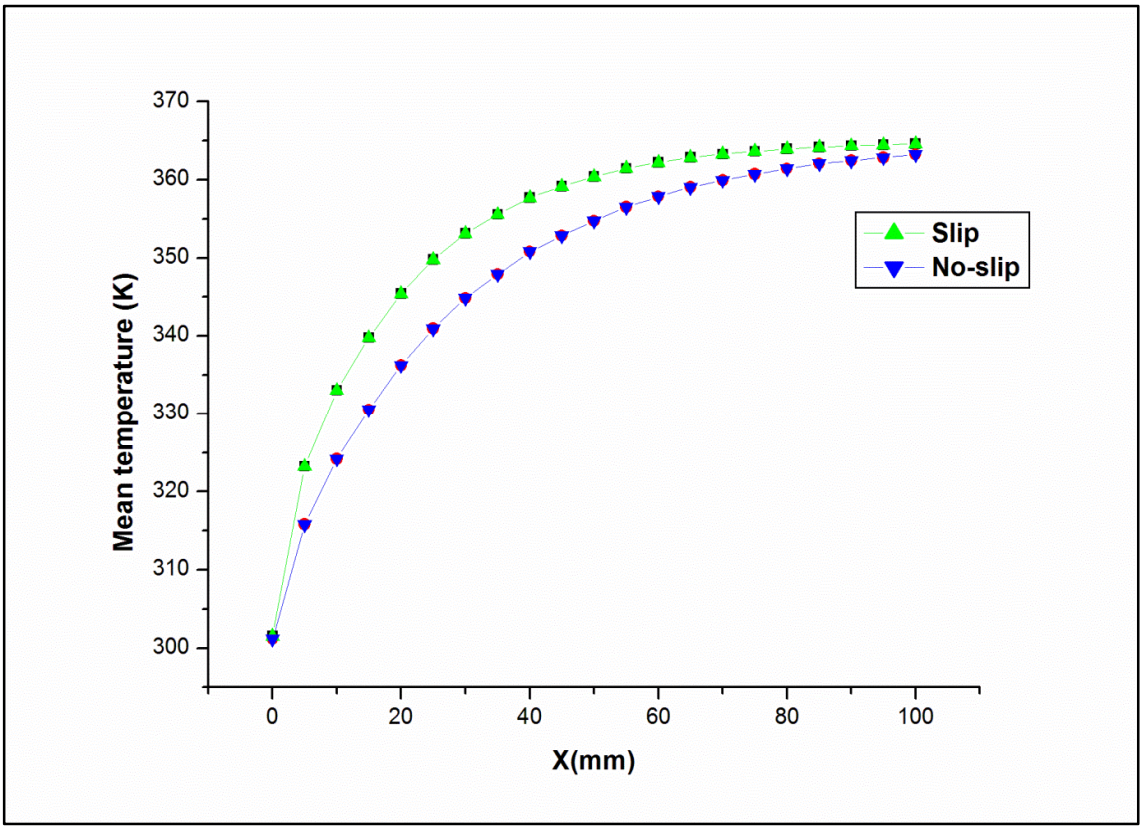

Fig 5.24 Variation of Mean temperature as function of length of mirochannel.

It can be depicted from the above fig.5.24 that the mean temperature of liquid reaches the surface temperature exponentially for isothermal condition. Due to the effect of slip the difference between the mean temperature and surface temperature is less but for no-slip the difference is quite large.

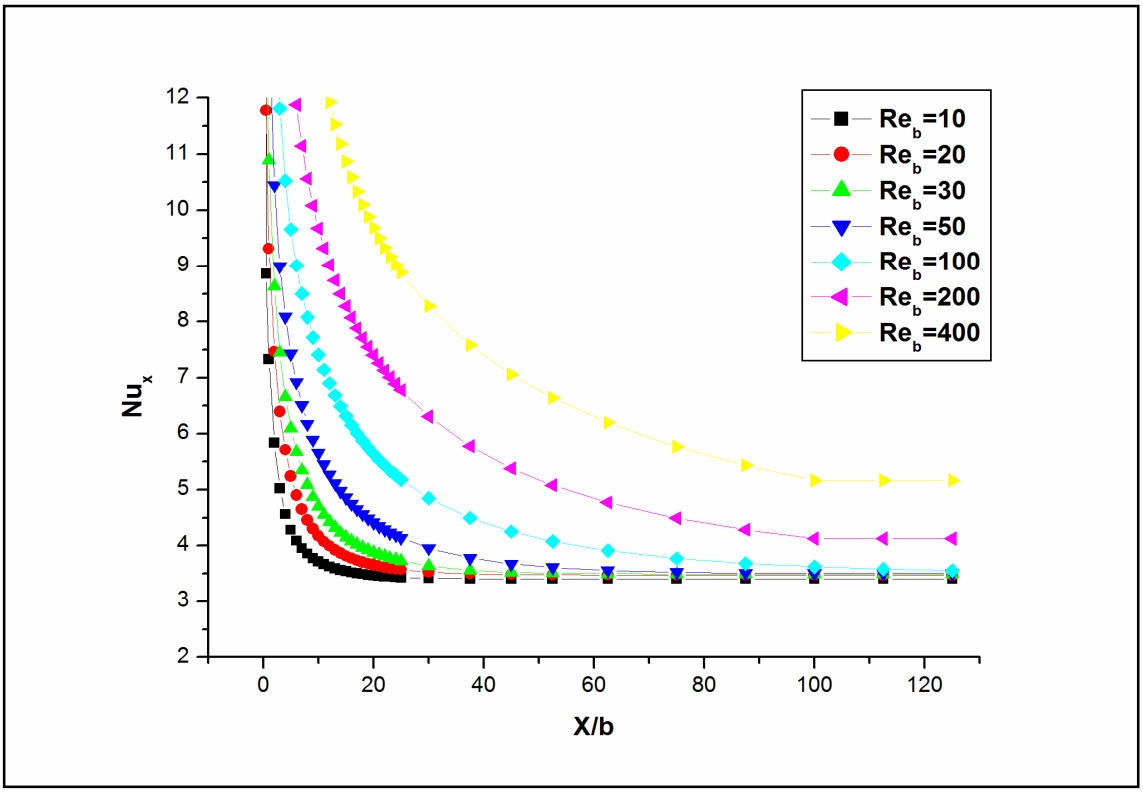

Fig 5.25 Variation of a non-dimensional Nusselt number against non-dimensional x/b for different values of Reynolds number.

The fig 5.25 shows the variation of a non-dimensional Nusselt number against non-dimensional x/b for different values of Reynolds number. The Reynolds number was defined for the width of the microchannel i.e. b. It was found that Nusselt number increase as the Reynolds number increases; since it is a function of Reynolds number. The increase in Nusselt number was approximately between 0.6 to 0.8.The effect axial conduction was considered in calculating the Nusselt Number, which causes the Nusselt number to increase.

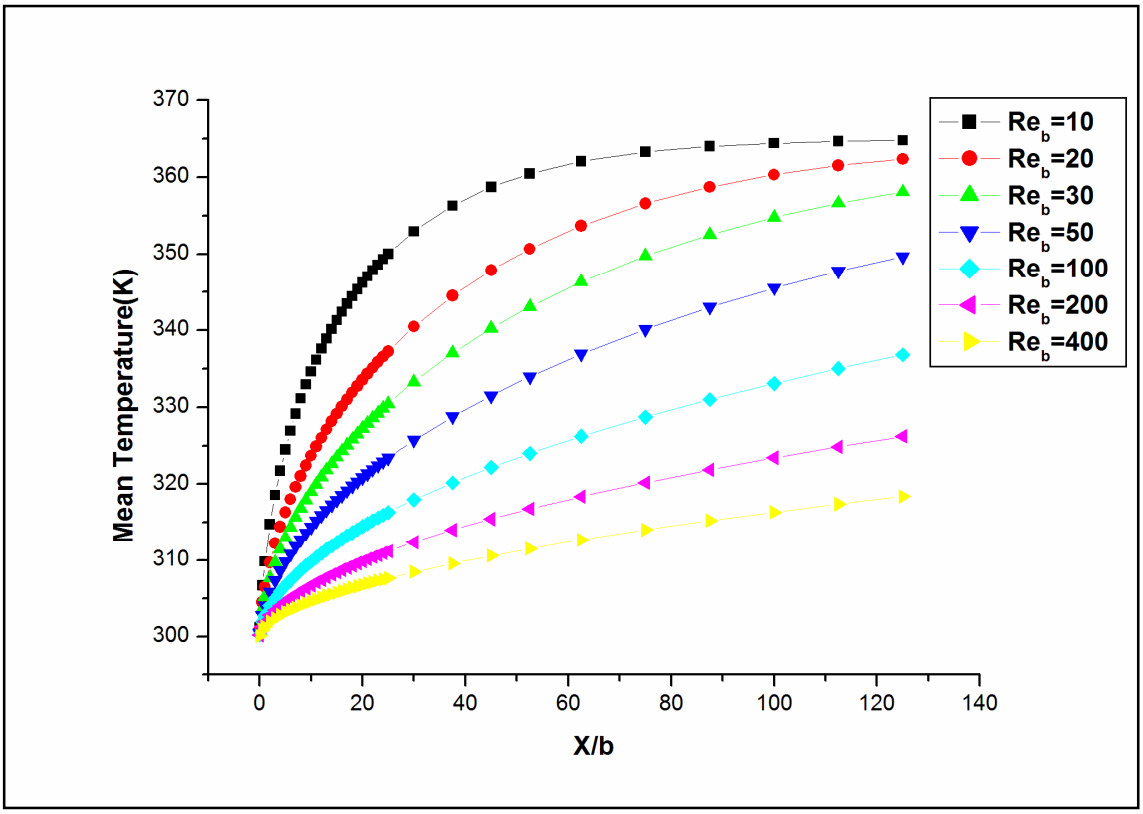

Fig 5.26Variation of mean temperature against non-dimensional number x/b for different values of Reynolds number.

The fig 5.26 shows the variation of mean temperature against non-dimensional number x/b for different values of Reynolds number. The trend of mean temperature is exponential in nature, the difference between the mean temperature and isothermal surface temperature increases as the Reynolds number increases.

Chapter 6

CONCLUSIONS AND FUTURE SCOPE

CONCLUSIONS AND FUTURE SCOPE

In this chapter the salient accomplishments and major conclusions of this work are summarized and recommendations for the future are made.

6.1 CONCLUSIONS

Keeping in view of its immense significance, this article is focused on the simulation and analysis of the microchannel flow. The narration of the microchannel flow behavior should contribute to the theoretical understanding of such flows. In Microchannel the heat transfer coefficient increases with slip flow considering axial conduction. The Nusselt remains constant in the fully developed region. Due to slip at the wall the shear rates is very small. In microchannel, the velocity in the radial direction is small in comparison with that in the axial direction. Flattening in the velocity profile is a phenomenon that has been found on the basis of one-dimensional flow problem, and it owes to the small scale of the dimensions of the microchannels involved. Slip velocity is a decreasing function of the axial dimension; hence, the channel after a certain length behaves as a minichannel, that is, channel with micro dimension but with no-slip condition. The non-linearity in pressure distribution with decreasing Reynolds number for a microchannel flow may cause compressibility effect. The slip effect reduces the friction in microchannel flow hence fluid can be driven through it with a lesser power consumption than in comparison to the flow through macro or mini-channel.

6.2 FUTURE SCOPE OF THE WORK

• Modeling and Simulation of slip velocity and temperature jump for gas flow in Microchannel

• Validation of CFD model with the Analytical solution.

REFERENCE

[1] S.S. Mehendale, A.M. Jacobi, R.K. Shah. Appl. Mech. Rev.,**2003;** 53, 175–193.

[2] S.G. Kandlikar,W.J. Grande. Heat Transfer Eng., **2003;** 24(1),3–17.

[3] S. Colin. Microfluidique, Lavoisier – Herm`es Science Publications:Paris, **2004**.

[4] C.B. Sobhan, S.V. Garimella. Microscale Thermophys. Eng.,**2001;** 5, 293–311.

[5] B. Palm. Microscale Thermophys. Eng., **2001;** 5, 155–175.[6] M. Gad-el-Hak. J. Fluids Eng., **1999;** 12, 5–33.

[7] G. Karniadakis, A. Beskok, N. Aluru. Microflows and Nanoflows Fundamentals and simulation, Springer: Los Angeles, CA, **2004**.

[8] C. Brodman. Untersuchungen ueber Reibungkoeffizienten zuFluessigkeiten. Dissertation, Goettingen, **1891**.

[9] C.L.M.H. Navier. Bull. Soc. Philomath., **1823;** 75, 177–183.

[10] J. Traube, S.H. Whang. Z. Phys. Chem. A, **1928;** 138,102–122.

[11] E. Schnell. J. Appl. Phys., **1956;** 27(1), 1149–1152.

[12] P. Debye, R.L. Cleland. J. Appl. Phys., **1959;** 30, 843–849.

[13] C. Chen. J. Micromech. Microeng., **2004;** 14, 1091–1100.

[14] D.C. Tretheway, C.D. Meinhart. Phys. Fluids, **2002;** 14(3),L9–L12.

[15] C.-H. Choi, J. Westin, K. Breuer. Phys. Fluids., **2003;** 15,2897–2902.

[16] T.D. Blake. Colloids Surf., **1990;** 47, 135–145.

[17] E. Ruckenstein, P. Rajora. Colloid Interface Sci., **1983;** 96,488–491.

[18] O.I. Vinogradova. Int. J. Miner. Process., **1999;** 56, 31–60.

[19] J.R. Phillip. J. Appl. Math. Phys., **1972;** 23, 353–372.

[20] P. deGennes. Langmuir, **2002;** 18, 3413–3414.

[21] J. Tyrrell, P. Attard. Langmuir, **2002;** 18, 160–167.

[22] G. Batchelor. An Introduction to Fluid Dynamics, Cambridge University Press: England, **1967**.

[23] P. Tabeling. In Proceedings 14th Australian Fluid Mechanics Conference, Adelaide, **2001**.

[24] C. Choi, K. Johan, A. Westin, K.S. Breuer. Proceedings IMECE200, New Orleans, **2002**.

[25] W.F. Ames. Non-linear Partial Differential Equations in Engineering, Vol 1, Academic Press: New York, **1967**.

[26] M.P. Arnal, D.J. Georing, J.A.C. Humphrey. J. Fluids Eng.**1991;** 113, 384–398.

[27] C.A.J. Fletcher. Springer Ser. Comput. Phys., **2000;** 1,362–368.

[28] S. Thakur, W. Shy. Numer. Heat Transfer Part B, **1993;** 24,31–55.

[29] A. Mukhopadhyay, G. Biswas, T. Sundarajan. Int. J. Numer.Methods Fluids, **1992;** 14, 1473–1484.

[30] R.R. Hwang, C. Yao. J. Fluids Eng., **1997;** 119, 512–518.

[31]Guyh Dituba Ngoma, Fouad Erchiqui, Heat flux and slip effects on liquid flow in a microchannel, International Journal of Thermal Sciences, Volume 46, Issue 11, November 2007,

[32]Journal of Micromechanics and Microengineering Volume 13 Number 5 Junemo Koo and Clement Kleinstreuer 2003 J. Micromech. Microeng. **13** 568 doi:10.1088/0960-1317/13/5/307 Liquid flow in microchannels: experimental observations and computational analyses of microfluidics effects